Impact of stalk on directly driven inertial confinement fusion implosions

M. Gatu Johnson (ID), P. J. Adrian (ID), K. S. Anderson, B. D. Appelbe, J. P. Chittenden, A. J. Crilly, D. Edgell, C. J. Forrest, J. A. Frenje (ID), V. Yu. Glebov (ID), B. M. Haines (ID), I. Igumenshchev, D. Jacobs-Perkins (ID), R. Janezic, N. V. Kabadi, J. P. Knauer, B. Lahmann, O. M. Mannion (ID), F. J. Marshall, T. Michel (ID), F. H. Séguin, R. Shah, C. Stoeckl, C. A. Walsh (ID), and R. D. Petrasso (ID)

COLLECTIONS

Paper published as part of the special topic on Papers from the 61st Annual Meeting of the APS Division of Plasma Physics

Note: This paper is part of the Special Collection: Papers from the 61st Annual Meeting of the APS Division of Plasma Physics.

View Online   Export Citation   CrossMark

ARTICLES YOU MAY BE INTERESTED IN

Mixing in ICF implosions on the National Ignition Facility caused by the fill-tube
Physics of Plasmas **27**, 032703 (2020); https://doi.org/10.1063/1.5125599

Three-dimensional signatures of self-similarity in a high-energy-density plasma shear-driven mixing layer
Physics of Plasmas **27**, 032701 (2020); https://doi.org/10.1063/1.5122980

The experimental investigation of the hohlraum energetics of two-entrance holes spherical hohlraum at the 100 kJ level laser facility
Physics of Plasmas **27**, 032702 (2020); https://doi.org/10.1063/1.5136274

Impact of stalk on directly driven inertial confinement fusion implosions

M. Gatu Johnson,[1,a] (iD) P. J. Adrian,[1] (iD) K. S. Anderson,[2] B. D. Appelbe,[3] J. P. Chittenden,[3] A. J. Crilly,[3] D. Edgell,[2]
C. J. Forrest,[2] J. A. Frenje,[1] (iD) V. Yu. Glebov,[2] (iD) B. M. Haines,[4] (iD) I. Igumenshchev,[2] D. Jacobs-Perkins,[2] (iD) R. Janezic,[2]
N. V. Kabadi,[1] J. P. Knauer,[2] B. Lahmann,[1] O. M. Mannion,[2] (iD) F. J. Marshall,[2] T. Michel,[2] (iD) F. H. Séguin,[1] R. Shah,[2]
C. Stoeckl,[2] C. A. Walsh,[3] (iD) and R. D. Petrasso[1] (iD)

AFFILIATIONS

[1]Massachusetts Institute of Technology, Cambridge, Massachusetts 02139, USA
[2]Laboratory for Laser Energetics, University of Rochester, Rochester, New York 14623, USA
[3]Centre for Inertial Fusion Studies, The Blackett Laboratory, Imperial College, London SW7 2AZ, United Kingdom
[4]Los Alamos National Laboratory, Los Alamos, New Mexico 87545, USA

Note: This paper is part of the Special Collection: Papers from the 61st Annual Meeting of the APS Division of Plasma Physics.
[a]Author to whom correspondence should be addressed: gatu@psfc.mit.edu

ABSTRACT

Low-mode asymmetries have emerged as one of the primary challenges to achieving high-performing inertial confinement fusion (ICF) implosions. In direct-drive ICF, an important potential seed of such asymmetries is the capsule stalk mount, the impact of which has remained a contentious question. In this paper, we describe the results from an experiment on the OMEGA laser with intentional offsets at varying angles to the capsule stalk mount, which clearly demonstrates the impact of the stalk mount on implosion dynamics. The angle between stalk and offset is found to significantly impact observables. Specifically, a larger directional flow is observed in neutron spectrum measurements when the offset is toward rather than away from the stalk, while an offset at 42° to the stalk gives minimal directional flow but still generates a large flow field in the implosion. No significant directional flow is seen due to stalk only. Time-integrated x-ray images support these flow observations. A trend is also seen in implosion yield, with lower yield obtained for offsets with a smaller angle than with a larger angle toward the stalk. Radiation hydrodynamic simulations using 2D DRACO and 2D/3D Chimera not including the stalk mount and using 2D xRAGE including the stalk mount are brought to bear on the data. The yield trend, the minimal directional flow with stalk only, and the larger flow enhancement observed with the offset toward the stalk are all reproduced in the xRAGE simulations. The results strongly indicate that the stalk impact must be considered and mitigated to achieve high-performing implosions.

Published under license by AIP Publishing. https://doi.org/10.1063/1.5141607

I. INTRODUCTION

Inertial confinement fusion (ICF) experiments aim to achieve fusion energy gain by spherically imploding a small (mm-scale) deuterium–tritium (DT) filled target using lasers, either indirectly using a hohlraum to convert the laser energy to x-rays,[1] or with the laser light directly incident on the target.[2] Independent of the approach, symmetric implosion of the target is critical to achieving the required pressures for high-performing experiments.[3] Low-mode asymmetries have emerged as a primary challenge to achieving high-gain ICF implosions[4–6] and have been the subject of significant recent work (e.g., Refs. 7–20). Low-mode asymmetries have been found to be seeded by factors external to the imploding target, including the engineering features used to support the target,[21–25] target offsets,[26] and

laser drive asymmetry,[13,27,28] and are also known to seed directional, non-thermal flows in the assembled fuel, which can be diagnosed through their impact on measured neutron energy spectra (see, e.g., Ref. 8).

A major outstanding question in the context of low-mode asymmetries concerns the impact on direct-drive ICF experiments of the stalk holding the target. Typically, 17-μm diameter silicon-carbide (SiC) stalks attached with glue spots (Fig. 1) are used to hold the targets in the chamber.[15,21] The impact of the stalk mount on the performance of direct-drive implosions has previously been discussed in, e.g., Refs. 13, 21, and 22, with varying conclusions. In Ref. 21, 2D simulations predicted an ∼50% reduction in yield due to the stalk mount for 27-μm thick plastic shell capsules shot with a shaped laser pulse.
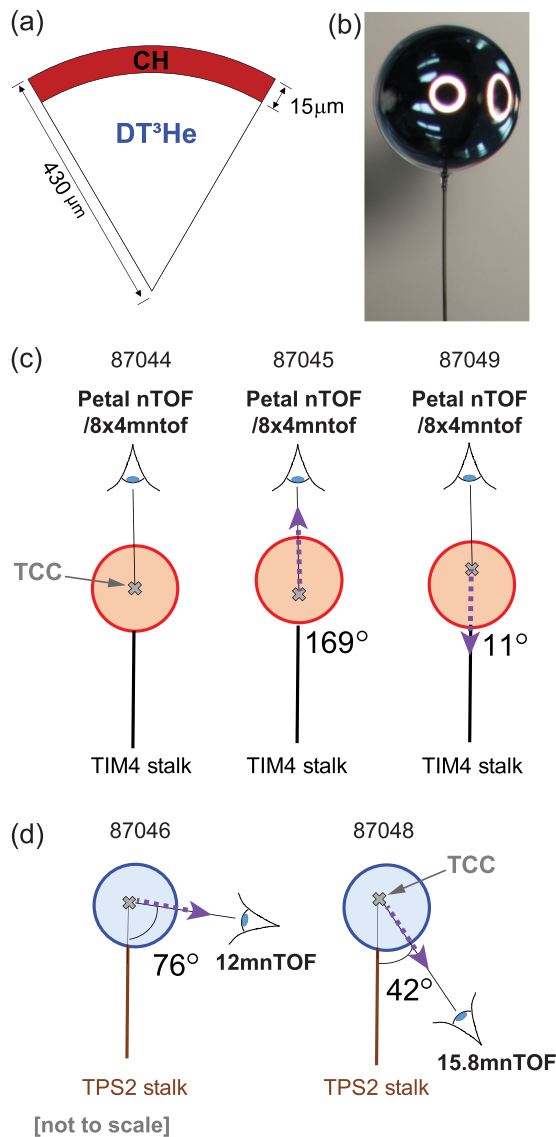
FIG. 1. Nominal experiment geometry. Target dimensions are shown in (a), a picture of the target used for shot 87048 in (b), and cartoons (not to scale) of the setup geometry for targets fielded on the TIM4 and TPS2 target positioners in (c) and (d), respectively. The cartoons show the TCC as a gray cross, the offset direction with a purple dashed arrow, and the nTOF detector with maximum expected flow signature in each case as an eye. For the offset shots, the as-shot angles [as measured using high-speed video (HSV)] between the stalk and the offset directions are also indicated. Please note that targets are centered on the stalk for all shots; the offsets are exaggerated in the cartoon for illustration purposes only.

The same simulation tool was later used to predict a significantly reduced impact on yield (7% vs 21% reduction) with a smaller glue spot compared to with a larger glue spot for 20-μm thick plastic shell capsules shot with a 1-ns square laser pulse.[13] This difference was not seen in experiments, which led to the conclusion that the stalk mount did not significantly impact the performance of these capsules.[13] In contrast, inclusion of the stalk in 3D simulations was required to

explain data from a separated reactant experiment.[22] In this case, the stalk was found to significantly impact the mixing of the shell material into the central cavity for 15-μm thick plastic targets shot with a 1-ns square laser pulse, and good agreement between simulated and measured yields was obtained with the inclusion of the stalk in the 3D simulations. Recent work[15,20] suggests the significant impact of the stalk on implosion dynamics and the flow field in the burning fuel. This raises the question of exactly how the stalk perturbs the implosion and what the stalk impact is on signatures of implosion asymmetry. The simulations presented in Ref. 21 predict that a jet of the shell material will be injected by the stalk that will then penetrate all the way through the central cavity and blow out through the shell on the opposite side. This picture of the stalk impact has never been experimentally validated.

The goal of the effort described in this paper was to further elucidate the impact of the stalk mount on implosion dynamics and to quantify its contributions to asymmetry signatures in direct-drive ICF experiments. This is achieved through comparison of signatures in yield, flow, T_{ion}, and x-ray imaging data from implosions on the OMEGA laser[29] with intentional offsets at varying angles to the stalk. The work points to a strong impact on implosion signatures of the stalk-offset angle. The maximum directional flow of the burning fuel is observed with the offset directly toward the stalk, while significantly smaller flow is seen with the offset away from the stalk. No significant directional flow is seen due to stalk only. Equivalently, a larger flow enhancement in the broadening of measured neutron energy spectra is also seen when the offset is toward rather than away from the stalk. Interestingly, minimal directional variations in neutron spectral broadening due to flows are seen with the offset at 42° to the stalk. Yield is also seen to trend with the stalk-offset angle, with a larger reduction in yield for offsets with a smaller angle to the stalk. Asymmetries in time-integrated x-ray images are seen to be sensitive to the angle between the offset and the stalk as well. Some of these trends are also seen in 2D simulations. From this work, it is very clear that the stalk strongly impacts implosion dynamics. This suggests that the stalk mount is the systematic asymmetry seed hypothesized in Ref. 30 to degrade the performance of cryogenically layered OMEGA DT implosions. The stalk mount is clearly a factor that must be considered, and its impact mitigated, to achieve higher-performing implosions.

This paper is organized as follows: Sec. II gives an introductory overview of the experiments, including details of the experimental setup and basic performance parameters. In Sec. III, three different simulations brought to bear on these experiments are discussed. As will be shown, none of the simulation tools used capture all effects known to be at play in the experiments; therefore, it is important to study results from all in an attempt to understand the influence of the various effects. In Sec. IV, the impact of the stalk on observables is highlighted, including contrasting experimental measurements to simulated results. In this section, we clearly demonstrate the signatures of the stalk mount in the data. Section V briefly summarizes the results presented in Sec. IV and discusses how the stalk impacts the implosions; while this cannot be conclusively established based on the present results, two hypotheses for the stalk-offset dynamics are presented. Finally, Sec. VI concludes the paper.

II. OFFSET TARGET EXPERIMENTS

The experiments discussed in this paper were designed with the explicit goal of testing the impact of the stalk mount on the flow field

TABLE I. Laser and target parameters for the five individual implosions performed as part of this experiment. Note that in addition to the CH shell thickness, there is also a 0.1 μm Al coating to prevent fill gas leakage. The $4\pi\Delta$ wall is a measurement of wall thickness variations around the target.

Shot	Shot description	Laser energy (kJ)	Outer diameter (μm)	CH shell thickness (μm)	$4\pi\Delta$ wall (μm)	Glue spot diameter (μm)	Glue spot length (μm)	DT fill (atm)	^{3}He fill (atm)
87044	Sym. Ref.	27.2	868	14.2	0.3	78.89	57.97	12.4	7.8
87045	Offset toward Petal nTOF	27.1	862	14.9	0.6	74.06	48.31	12.5	7.9
87046	Offset toward 12 m nTOF	27.1	864	14.3	0.2	74.06	83.74	12.6	8.0
87048	Offset toward 15.8 m nTOF/3dp2	27.3	858	14.5	0.4	80.50	95.01	12.6	7.9
87049	Offset away from Petal nTOF	27.5	868	14.1	0.1	Re-glued (fell off stalk)		12.2	7.5

in direct-drive ICF implosions. Flows in the burning fuel can be inferred from peak shifts[31–33] and line-of-sight (LOS) variations in broadening[34,35] of measured neutron energy spectra.[36,37] An apparent ion temperature (henceforth referred to as T_{ion}) is inferred from the neutron spectral broadening, and this T_{ion} will have contributions both from thermal T_{ion} and from flow variance in the LOS of the detecting neutron spectrometer.[34] [We note that the T_{ion} analysis assumes Maxwellian ion distributions; deviations from Maxwellian due to long ion–ion mean free paths and tail ion depletion[38] may lead to a reduced peak width and, consequently, underestimated T_{ion};[39] however, any such effects present in these implosions (which have estimated Knudsen numbers $\sim$0.1) are expected to impact all LOS equally and thus not impact conclusions drawn from LOS asymmetries.]

Five implosions were executed as part of this experiment, of which one was a symmetric reference case with the target positioned as close as possible to the target chamber center (TCC), and four had intentional 40-μm offsets at different angles to the capsule stalk mount and with directions intended to maximize flow signatures in different OMEGA neutron time-of-flight (nTOF) neutron spectrometers[33,40–42] (Fig. 1). Offsets are expected to setup a predictable, directional flow field in the implosions, and varying the stalk-offset angle tests how much the stalk perturbs that flow field. The 40-μm magnitude for the offsets was selected to balance the expected signatures of the offset in LOS variations in T_{ion} and in reduction in neutron yields. Pre-shot 3D ASTER[11,12] simulations predicted a 2.7 keV LOS variation in T_{ion} and 70% yield reduction for 40-μm offsets, not considering the stalk mount; larger offset would give larger LOS variations, but they would be harder to measure due to lower yield.

Nominally, 870-μm outer diameter targets with 15-μm thick shells were used for the experiments (the shell thickness was also selected to maximize flow signatures; for comparison, only a 1.6 keV LOS variation in T_{ion} was predicted from ASTER for 20-μm thick targets). The targets were filled with a mixture of D:T:^{3}He gas, to give DT neutrons for the flow measurements and D^{3}He protons for directional ρR measurements. All targets were held with standard 17-μm SiC stalks but using two different target positioners: TIM4 at θ, $\varphi = 63°$ and 342° and TPS2 at θ, $\varphi = 37°$ and 90°. Target parameters for all implosions are summarized in Table I. Note that the target for 87049 fell off the stalk during the shot day and had to be re-glued before shot; this means that the glue spot is not characterized for this target and that it has an additional small residual glue spot from the initial mount. From x-ray images (Fig. 9), we estimate that this residual glue is at $\sim$120° from the stalk.

Accurate positioning of the targets was achieved using a system of two high-speed video (HSV) cameras. This system also outputs numbers for the position of the target at shot time. For comparison, target positions were also inferred from a system of x-ray pinhole cameras (XRPC), based on time-integrated x-ray images from the implosion;[43] both HSV and XRPC numbers are summarized in Table II and are found to be generally very consistent. We note that the positioning is done relative to a recent TCC reference shot;[43] for the present experiment, this reference shot was taken on the previous day, and any drifts are expected to be negligible.

All targets were imploded with a 1-ns square laser pulse using all 60 OMEGA laser beams. Optimal drive conditions (expected time-averaged illumination non-uniformity better than 2% rms,[44] not

TABLE II. Target positioner and offset (as measured using high-speed video and x-ray pinhole cameras, respectively) for the five individual implosions performed as part of this experiment.

Shot	Target positioner	Offset-stalk angle	High speed video			X-ray pinhole cameras		
			Offset magnitude (μm)	Offset θ (°)	Offset ϕ (°)	Offset magnitude (μm)	Offset θ (°)	Offset ϕ (°)
87044	TIM4	Sym. ref.	8.3	119.0	45.3	15.8	158.3	57.7
87045	TIM4	169°	40.8	120.8	151.1	44.8	115.7	168.0
87046	TPS2	76°	37.4	88.6	158.8	36.0	89	160.5
87048	TPS2	42°	41.5	65.6	48.3	34.0	63.7	53.7
87049	TIM4	11°	41.4	69.6	352.2	39.9	70.8	356.3

considering offsets or stalk) were obtained through the use of distributed phase plates, two-dimensional smoothing by spectral dispersion,[45] and polarization smoothing.[46] The as-shot beam balance was also characterized through measurements of energy and timing (using the harmonic energy detector and the P510 streak cameras, respectively) for each beam[47,48] and found to be within 1.5%–1.8% rms depending on shot (all beams used nominally the same energy; the laser intensity asymmetry illustrated in Fig. 2 arises because of the capsule offsets). These measurements are done outside of the target chamber and have to be corrected for transmission through the final optics assembly and blast shields but are expected to be accurate for these shots due to blast shield replacements prior to the preceding shot day. Precision beam pointing was done on the preceding shot day; while it may have drifted slightly overnight, it is expected to stay the same throughout our five-shot series with rms better than 20 μm.[29]

The combined effect of HSV-inferred offset and the as-shot beam energy balance on the target illumination uniformity as calculated using VisRad[49] for each implosion is illustrated in Fig. 2. According to these static calculations, the offsets are equivalent to a drive asymmetry (max–min)/min for these implosions of ~25%. Note, however, that these calculations do not consider smoothing due to cross-beam energy transfer (CBET), which has been recently found to decrease the effect of offsets on implosion performance.[50] Figure 2 also shows the locations of each of the nTOF detectors used in these experiments. The Petal, 15.8 m nTOF, 12 m nTOF, 15.9 m MCP nTOF, and 10.4 m PD040 are all used to measure directional T_{ion}. Petal also measures peak shifts, from which directional velocities are inferred.[51] Not shown in Fig. 2 is the 8×4 m nTOF detector, which shares LOS with Petal.[52] This detector measures the deuterium-deuterium (DD) neutron peak, from which an additional independent directional velocity measurement is obtained. The black stars in Fig. 2 represent the stalk direction, while the purple stars represent the offset direction for each shot. The laser intensity curves clearly show how the on-target intensity is minimized in the direction of the offset and maximized away from the offset in each case. Note also how the offset is toward Petal for shot 87045, toward 12 m nTOF for 87046, toward 15.8 m nTOF for shot 87048, and away from Petal for shot 87049.

In addition to the nTOF flow measurements, a number of other diagnostics were also employed to characterize the effect of offsets and stalks on these implosions. These include time-integrated x-ray imaging using the gated monochromatic x-ray imager[53] (GMXI) with $\theta = 96°$, $\phi = 54°$ and time-resolved in-flight x-ray imaging using two framing cameras in TIM2 and TIM5 with $\theta = 37°$, $\phi = 162°$ and $\theta = 101°$, $\phi = 270°$, respectively. The goal with the time-resolved x-ray imaging was to get an x-ray measurement of the target motion during the implosion for comparison with the nuclear measurements, using the method described in Ref. 54. This also involved fielding a solid (non-imploding) CH sphere as a time-resolved position reference (shot 87050). Five charged particle spectrometers were also fielded to measure the LOS-dependent proton spectra from these implosions: the magnetic recoil spectrometer (MRS,[55] θ, $\varphi = 119°$, 308°), two charged particle spectrometers[56] (CPS1 with θ, $\varphi = 63°$, 198° and CPS2 with θ, $\varphi = 37°$, 18°), and two wedge range filter spectrometers (WRF,[57] fielded in TIM3 with θ, $\varphi = 143°$, 342° and P2NDI with θ, $\varphi = 58°$, 54°). Knock-on protons (KO-p), from DT-n elastically scattering in the CH shell, and D³He-protons from reactions between D and ³He in the fuel contribute to the measured proton spectra (see Ref. 20 for an
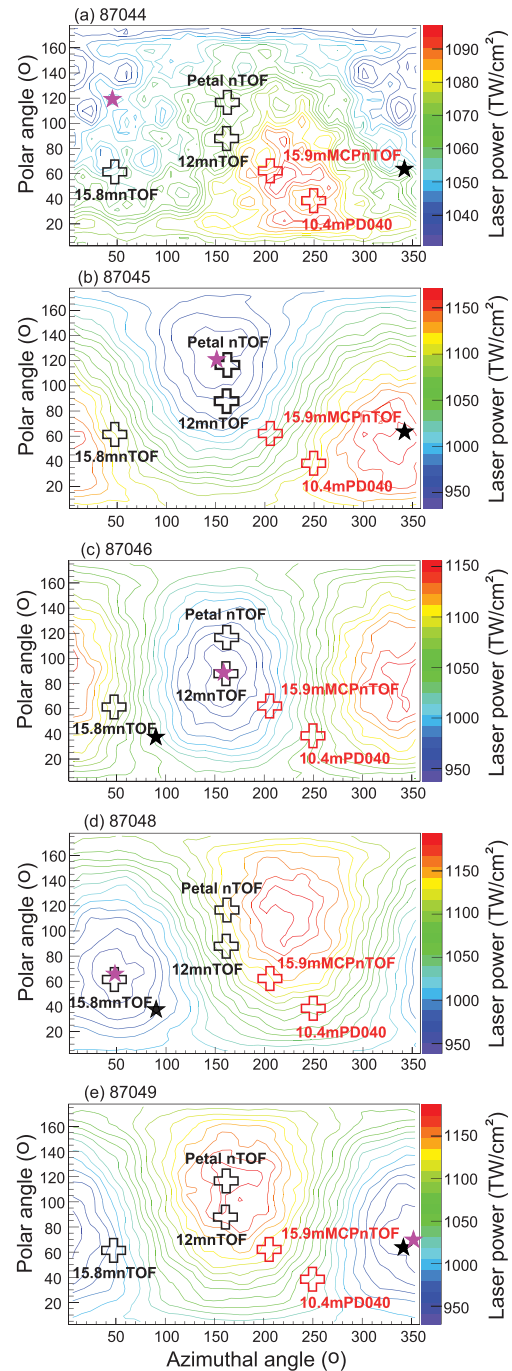
FIG. 2. VisRad-calculated drive asymmetry equivalent of the offsets, considering the as-shot laser drive but not the stalk and not any cross-beam energy transfer (CBET), for (a) symmetric reference shot 87044, (b) shot 87045 with the offset away from the stalk, (c) shot 87046 with the offset at 76° to the stalk, (d) shot 87048 with the offset at 42° to the stalk, and (e) shot 87049 with the offset toward the stalk. In each panel, the five nTOF detector directions are indicated with plus signs, the stalk direction with a black star, and the offset direction with a purple star. The (max-min)/min drive equivalent is 6.8% for shot 87044, 26.1% for shot 87045, 23.5% for shot 87046, 27.4% for shot 87048, and 28.1% for shot 87049.

TABLE III. Summary of performance parameters. The DT-n yield is the average of measurements with 15.8 m nTOF, 12 m nTOF, and 10.4 m PD040, with the standard deviation as the uncertainty (the absolute DT yield uncertainty is 5%). T_{ion} is the average from the five reporting detectors, with the weighted average uncertainty. The D^3He-p yield and the ρR are the averages measured with CPS1, CPS2, MRS, and WRFs in TIM3 and P2NDI, again with the standard deviation as the uncertainty. Bang times (± 50 ps uncertainty) and burn durations (corrected for the NTD response and thermal broadening[60]) are measured using NTD.

Shot	DT-n yield ($\times 10^{12}$)	D^3He-p yield ($\times 10^9$)	Average DT T_{ion} (keV)	DT T_{ion} st. dev. (keV)	Bang time (ps)	Burn duration (ps)	Average ρR (mg/cm^2)
87044	6.9 ± 0.1	4.9 ± 1.5	5.64 ± 0.08	0.15	1397	114	34.1 ± 2.4
87045	10.1 ± 0.3	5.2 ± 1.4	5.98 ± 0.08	0.24	1455	111	34.3 ± 10.8
87046	8.7 ± 0.2	4.8 ± 1.3	6.16 ± 0.08	0.22	1422	106	35.6 ± 8.0
87048	8.0 ± 0.1	4.5 ± 1.2	5.99 ± 0.08	0.14	1436	110	34.1 ± 11.3
87049	7.1 ± 0.1	3.7 ± 0.4	6.36 ± 0.09	0.35	1419	119	26.2 ± 3.6

example spectrum). Shell ρR is inferred from the KO-p yield,[58] and total ρR from the D^3He-p energy downshift.[20,59] The proton spectrum measurements also give D^3He-p yield (Table III). The ρR measurements are discussed in Appendix A. Standard DT yield (nTOF) and burn history (neutron temporal diagnostic, NTD[60]) measurements were also obtained. Basic performance parameters for the five implosions are summarized in Table III. Note that given the best-estimate D:T:^{3}He fuel fill fractions of about 23%:53%:24%, the measured T_{ion}, and known DT and D^3He reactivities,[61] the measured D^3He yields are about a factor 2 higher than expected compared to the DT yields. This is currently believed to be due to fill fraction uncertainties; nominally identical implosions have previously been demonstrated to give DT and D^3He yields in excellent agreement with expectation.[20]

The stalk effect implications of the results will be discussed in Sec. IV.

The full-aperture backscatter calorimetry diagnostic[62] measured an absorption of 56% for the symmetric reference shot. For the offset shots, the measured numbers vary from 41% to 67% between individual detectors depending on whether the offset is toward or away from the diagnostic. It is believed that 56% is a representative absorption number for all implosions.

III. SIMULATIONS

Several different radiation-hydrodynamic simulation tools were brought to bear on these experiments to aid in interpretation of the results: 1D LILAC,[63] 2D DRACO,[64] 2D xRAGE,[22,65,66] and 2D and 3D Chimera,[67] with the latter initialized with 1D HYADES.[68] It is important to note that none of these tools capture all effects known to be at play in these experiments, which include (but are not limited to) capsule offsets, stalk, CBET, the as-shot beam balance, and shot-to-shot variations in capsule parameters. Of the simulations performed

for these experiments, only DRACO explicitly models CBET, only xRAGE considers the stalk mount in the simulation, and only Chimera considers 3D effects. In the discussion below, we discuss the known limitations of each code; these also become clear when contrasting the simulation results to measurements. For example, while CBET is likely to be important, the present DRACO simulations, which do not consider stalk mount, cannot capture the experimental observables. As will be shown, xRAGE, which does consider the stalk mount, comes closest to matching the measurements. Future simulations capable of simultaneously considering all these effects should be expected to better capture all experimental signatures.

The 1D LILAC simulations show that yield scales with target wall thickness in this CH shell thickness range, with lower shell thickness giving higher yield due to higher achieved implosion velocity with the same laser energy. According to these simulations, the impact on yield is $\sim 1.3\%$ per 0.1 μm shell thickness. It is important to point out in this context that the uncertainty in the measurement of shell thickness is 0.3 μm.

A. 2D DRACO

DRACO is an arbitrary Lagrangian-Eulerian structured mesh code. DRACO simulations of the present experiments were performed in 2D and included an explicit CBET model, using the methodology described in Ref. 69, and a non-local thermal conduction model using an implicit Schurtz–Nicolaï–Busquet model.[70] The DRACO results were post-processed with IRIS3D[71] for synthetic neutron spectrum observables. The DRACO simulations consider capsule offsets but not the stalk mount or other low-mode non-uniformities, e.g., power imbalance and beam mispointing, and are performed for all implosions. DRACO-simulated observables are summarized in Table IV.

TABLE IV. Results from 2D DRACO simulations. The max and min T_{ion} and flow in Petal LOS are obtained from IRIS3D post-processing of the DRACO output. Note that the max and min are calculated across the five nTOF LOSs available for the measurements and thus directly comparable to data.

Shot	DT-n yield ($\times 10^{13}$)	D^3He-p yield ($\times 10^9$)	Bang time (ns)	Max T_{ion} (keV)	Min T_{ion} (keV)	Flow in Petal LOS (km/s)
87044	1.25	1.86	1.459	2.88	2.88	13.9
87045	1.12	1.50	1.498			
87046	1.17	1.69	1.466	2.97	2.96	24.9
87048	1.15	1.60	1.472	3.03	3.01	25.0
87049	1.28	1.87	1.463	2.89	2.88	24.1

Comparing Table IV with Table III, we note that DRACO-simulated DT-n yields are higher than measured, while simulated D^{3}He-p yields and T_{ion}'s are lower. Simulated bang times are slightly later than measured. These observations are consistently explained with the DRACO-simulated implosion velocity being too low; further tuning of the simulation would be expected to improve the agreement. Laser imprint was also not modeled in these simulations, which is expected to further reduce fusion yields.[6,72] Consistent with LILAC, DRACO-simulated yields are also seen to scale with shell thickness, with the highest simulated yield obtained for the thinnest shell shot (87049). This is in spite of this shot having a 40-μm offset. To verify the impact of offset on yield, a series of DRACO simulations were also run varying the capsule offset for shot 87045. With no offset, the simulated yield for this implosion is 1.15×10^{13}, while with 60-μm offset, the yield is 1.07×10^{13}; this is only about a 7% reduction. With the measured 40.2-μm offset, the yield reduction is only 2% compared to the no-offset case. The small impact of offset on yield in these simulations is due to CBET compensating for the drive asymmetry introduced by the offset.[50] It is currently believed that DRACO overestimates this CBET-related asymmetry compensation by not including the effect of the stalk, from which the ablated plasma may block or redirect substantial portions of the incoming and outgoing beams on that side, thereby reducing the beam-to-beam interactions on the stalk side (this will be tested in future simulations).

B. 2D xRAGE

xRAGE is an Eulerian radiation-hydrodynamic code featuring adaptive mesh refinement (AMR), making it well suited for modeling the capsule stalk mount. The xRAGE simulations of the experiments described in this paper included hydrodynamics with SESAME tabular equations of state, laser ray-tracing using the Laboratory for Laser Energetics' Mazinisin package[73] from DRACO without CBET, multi-group radiation diffusion with OPLIB opacities, flux limited electronic and ionic thermal heat conduction, a three-temperature plasma treatment, and thermonuclear burn. Simulations were performed in 2D with a maximum AMR resolution of 0.25 μm and included accurate models for the glue spot used to attach the target to the stalk and for capsule surface roughness. Laser imprint was also considered. xRAGE simulations were only performed for shots 87044, 87045, and 87049 with the stalk and offset aligned along the same axis; including the stalk mount in modeling of 87046 and 87048 would require 3D geometry. Because of the 2D geometry, the intrinsic (as-shot) drive asymmetry is also not considered.

The results from the 2D xRAGE simulations are summarized in Table V. As can be seen, the simulated yields are 50%–100% higher than measured (compare Table III). A likely reason for this (based on previous results[22,74]) is 3D effects not captured in the 2D simulations, including the intrinsic drive asymmetry. Bang times and burn durations are in excellent agreement with measurements. T_{ion} and flow will be discussed further in Sec. IV.

xRAGE-simulated T_{ion} and density maps are shown in Fig. 3. These images very clearly show how the offset [down in Fig. 3(b), up in Fig. 3(c)] leads to a higher density away from the offset and an offset of the hot spot in the direction of the offset (consistent with the mode 1 perturbation picture from Ref. 8). Note that the stalk enters from the top in these images.

It is important to note that the xRAGE simulations of the experiments discussed here only consider the glue spot and not the stalk itself. Test problems have shown that in the xRAGE simulations, the impact of the stalk itself is minimal as it ablates very early on in the implosion. The simulations do account for the mass perturbation, laser shadowing, and variations in laser absorption introduced by the glue spot. According to xRAGE, the primary effect that seems to be important is the shadowing by the glue spot and the added mass due to the glue spot (the shell accelerates more quickly around the glue spot, so that a hole eventually forms between the glue spot and the rest of the shell, allowing a jet to penetrate into the fuel region). We note that while the xRAGE simulations point to the glue spot as the primary source of the stalk mount perturbation, in the present experiments, there is no way of separating the effect of the glue spot from the effect of the SiC stalk, and our results cannot conclusively distinguish between the impact from one or the other (this is further discussed in Sec. V).

C. 2D/3D Chimera

Chimera is an Eulerian-mesh code with capability to run in 1D, 2D, or 3D. Two different Chimera simulations were run for the present work: 2D and 3D. Chimera does not consider the capsule stalk mount and was used to simulate all five implosions. The 3D simulations were done with the same methodology as used in Refs. 15 and 20, initializing the 3D Chimera simulations post shock-breakout using output from 1D HYADES simulations with varying laser drive. The same baseline HYADES simulation was used to initialize the Chimera runs for all shots, which means that variations in capsule thickness are not considered in these simulations. The as-shot laser drive is however considered, including variations around the capsule within a shot and in total energy between shots. The results from the 3D Chimera simulations are summarized in Table VI. Yields are higher than from DRACO and xRAGE; the early bang time relative to the experiment (compare Table III) may indicate that the implosion velocity is slightly over-estimated in the simulation, leading to high inferred yield.

TABLE V. Results from 2D xRAGE simulations (BWTI represents a burn-averaged thermal temperature, not considering flow broadening).

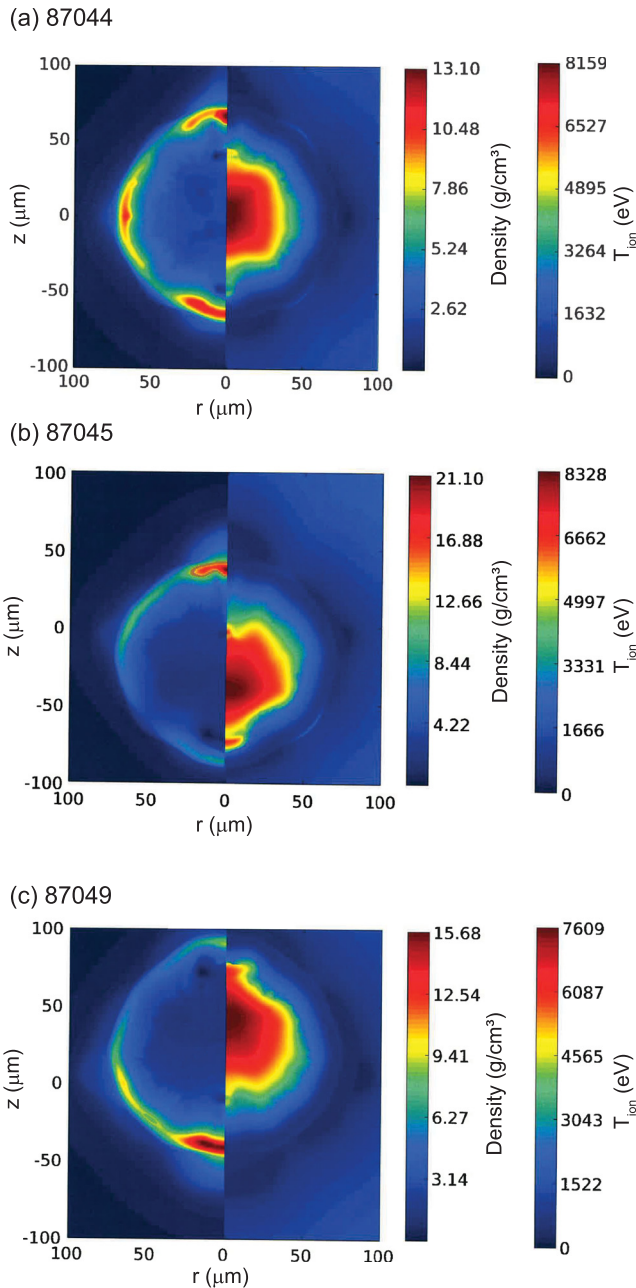| Shot	DT-n yield ($\times 10^{13}$)	Bang time (ns)	Burn duration (ps)	BWTI (keV)	DT T_{ion} parallel to stalk (keV)	DT T_{ion} perp. to stalk (keV)	Flow toward stalk (km/s)
87044	1.27	1.40	111	5.33	5.50	5.47	21
87045	1.53	1.44	110	5.69	6.30	5.81	−185
87049	1.46	1.42	116	5.36	6.36	5.69	186

FIG. 3. 2D xRAGE-simulated density (left) and T_{ion} (right) color maps at bang time for (a) shot 87044, (b) shot 87045, and (c) shot 87049. The stalk is entering from the top in each image.

TABLE VI. Results from the 3D Chimera simulations. The average T_{ion} is calculated over the experimental LOS used on the shot day and is directly comparable to the measured number in Table III.

Shot	DT-n yield ($\times 10^{13}$)	Bang time (ns)	Average T_{ion} (keV)	Flow in Petal LOS (km/s)
87044	3.70	1.319	5.88	−8.1
87045	2.78	1.313	6.18	176.7
87046	2.96	1.313	6.21	144.5
87048	2.63	1.316	6.08	−98.5
87049	2.63	1.312	6.31	−188.0

giving results closer to measured. The differences arise due to the different initialization of the two codes and indicate that some further tuning of the 2D simulations is required; updating the ion thermal transport modeling in the 2D simulations may bring the two methods into better agreement (flux limiter scans have shown that simulated T_{ion} depends strongly on the ion flux limiter). As for velocities and T_{ion} anisotropy, the 2D values are close to the 3D results. This suggests that the drive-phase lateral thermal smoothing is having a similar impact to the late-time 3D asymmetry. If both of these effects could be combined into one simulation, then the simulated velocity asymmetry would be expected to be lower.

IV. IMPACT OF STALK ON OBSERVABLES

The impact of the stalk on these implosions is determined by comparing data from implosions with different stalk-offset geometries. In this section, measured and simulated directional flows, T_{ion}, yield, and x-ray images are compared, and implications of the comparisons are discussed.

A. Flows

As mentioned in Sec. II, directional flows for these implosions were inferred from neutron spectrum peak shifts as measured using the Petal and 8 × 4 m nTOF detectors. These detectors, both of which are in the same LOS, are in the direction of the offset and opposite the stalk for shot 87045 and opposite both the offset and stalk for shot 87049 (see Fig. 1). Figure 4 shows measured and simulated flows as a function of offset projection in this nTOF LOS. The measured offset projection is calculated as the average of XRPC and HSV projected offsets with the error bar spanning the individual numbers from each of these methods; for the simulations, the projected HSV offsets are used.

The first thing to note from Fig. 4 is that a linear trend in flow with offset projection is expected if the stalk is not considered in the simulation [see Chimera results in Fig. 4(b)]. Generally, the measurements also follow a linear trend, but there are obvious deviations as will be discussed. Second, the inferred flow from nominally centered shot 87044 is consistent with zero (the weighted average of the two measurements is -4.4 ± 10.4 km/s) in spite of the measurement being made directly opposite the stalk. This is a very interesting observation on its own, indicating that the stalk itself does not seed a directional flow in the burning fuel. The measurement for 87044 is also in good agreement with the 2D xRAGE simulation including the stalk (red cross in Fig. 4). Third, comparing the flow magnitudes for the cases
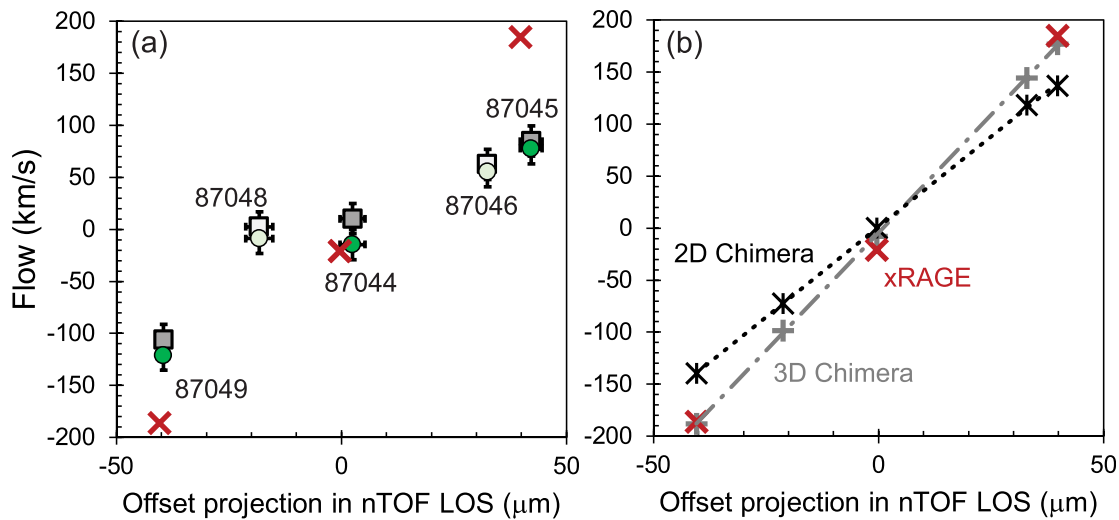
The HYADES initialization methodology is limited in that it does not consider transverse thermal smoothing. For this reason, 2D simulations that do consider transverse thermal smoothing were also run. These are full Chimera simulations with no HYADES initialization. The baseline T_{ion} obtained from the 2D simulations is significantly lower than T_{ion} from the 3D simulations, with the 3D simulations

FIG. 4. (a) Directional flow as measured with the Petal nTOF (green circles) and the 8 × 4 m nTOF (gray squares), sharing a single LOS. For Petal nTOF, the flow velocity is inferred from the DT neutron peak, while for 8 × 4 m nTOF, the flow velocity is inferred from the DD neutron peak. Light data points represent shots with the stalk in TPS2, while dark data points represent shots with the stalk held by TIM4. The measured offset projection is the average projection obtained using HSV and XRPC measured offsets, with the error bar spanning the range of using one or the other to calculate the projection. Also shown are the xRAGE-simulated directional flows in the Petal LOS (red crosses). (b) xRAGE and Chimera-simulated directional flows, plotted against projected HSV offsets. The xRAGE results are shown in both panels for easy comparison.

with the offset toward or away from the stalk, a significant difference is seen, with a weighted average flow magnitude of 81 ± 10 km/s for the case with the offset away from the stalk (87045) and 114 ± 10 km/s for the case with the offset toward the stalk (87049). This important difference is also backed up by T_{ion} observations as will be shown below, leading to the conclusion that the implosion is more perturbed in the case with the offset toward rather than away from the stalk. Finally, shot 87048 with the offset at 42° to the stalk (compare Fig. 1) clearly stands out from the overall trend. The measured flow magnitude for this shot is significantly smaller than expected based on the offset projection (the Petal and 8 × 4 m nTOF detector LOS is 121° from the offset direction for this shot, and the detectors will see 51% of a flow induced in the offset direction). This observation is also supported by T_{ion} data as will be discussed below, leading to the conclusion that directional flow is minimized in this configuration.

Comparing the measured flow magnitudes with simulations, it is clear that the DRACO simulations underestimate the flows (Table IV). As discussed above, this might be because the implosion velocity is not correctly captured in the DRACO simulations. Also the CBET calculation in DRACO may overestimate the asymmetry correction of the scattered light by omitting the stalk effect. 2D xRAGE is seen to overestimate the directional flows. A potential reason for this is the small residual offset in the experiment which is not along the stalk axis, which cannot be captured in the 2D simulations. Forcing axisymmetry in the simulation also tends to enhance any jetting that occurs along the axis of symmetry.[75] The 3D Chimera simulations also over-estimate the directional flow; this is believed to be due to transverse radiation transport not being considered in these simulations. The lack of CBET modeling in xRAGE and Chimera may also cause these codes to overpredict hot-spot flows.

B. T_{ion}

T_{ion} measurements for all reporting nTOF detectors are shown as a function of offset projection in each nTOF LOS in Fig. 5 (here, the offset is again taken as the average inferred from XRPC and HSV). Note that measurements are compared for individual detectors across shots instead of for individual shots across detectors to eliminate any questions about systematic calibration differences between the detectors (the detectors are periodically cross-calibrated to give the same answer on warm shots, which means that they would have any stalk impact calibrated out). Also shown in Fig. 5 are simulated T_{ion} values from 3D Chimera simulations (gray plus signs). As can be seen, a parabolic dependence is expected as a function of projected offset in the detector line-of-sight (although some deviations from this general behavior are seen in the 3D Chimera results, which do consider the as-shot laser drive). This parabolic trend arises because even though the flow is directional (Fig. 4), the flow variance and hence impact on T_{ion} are the same both parallel and antiparallel to the flow direction. The flow variance perpendicular to the flow direction (zero offset projection), on the other hand, is minimal, leading to minimal flow enhancement in measured T_{ion} in this direction.

Contrasting the measurements to the Chimera predictions, clear correlations can be seen between the T_{ion} measurements and the flow results discussed above (Fig. 4). In particular, shot 87045 with the offset away from the stalk shows a much smaller flow enhancement than shot 87049 with the offset toward the stalk, consistent with the observation from the directional flow. This can be seen in both the Petal and 12 m nTOF LOSs [Figs. 5(a) and 5(b)]. The offset for shot 87048 (at 42° to the stalk) is directly toward 15.8 m nTOF [Fig. 5(c)], leading to maximum expected T_{ion} for this shot in this LOS. This is not born out in the data, again consistent with the flow observations, which also showed lower-than-expected directional flow for this shot. In this context, it is interesting to look at the average and standard deviations in
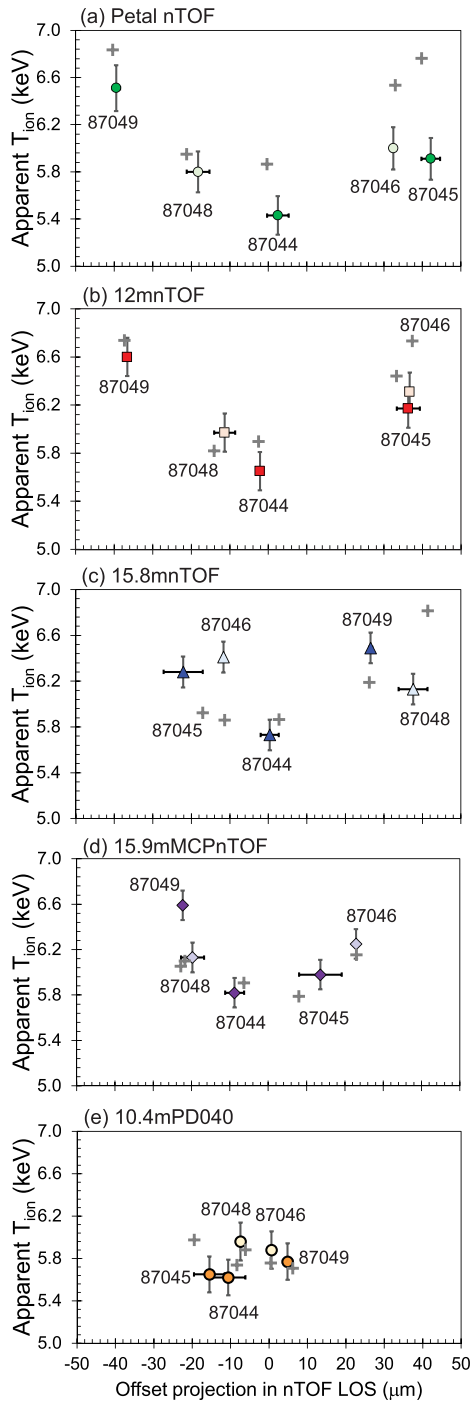
FIG. 5. Measured apparent T_{ion} as a function of offset projection in the nTOF line-of-sight for (a) Petal nTOF, (b) 12 m nTOF, (c) 15.8 m nTOF, (d) 15.9 m MCP nTOF, and (e) 10.4 m PD040 (see Fig. 2 for nTOF locations). Light symbols represent shots with the stalk in TPS2, while dark symbols represent shots with the stalk in TIM4. The offset projection is the average projection obtained using HSV and XRPC measured offsets, with the error bar spanning the range of using one or the other to calculate the projection. Gray plus signs represent 3D Chimera-simulated T_{ion}, using HSV offsets.

T_{ion} measured for all shots (Table III). With only five LOSs per shot, there is a possibility that an imposed asymmetry will be undersampled, leading to an artificially low standard deviation in T_{ion}. Full sampling of an asymmetry requires coverage both perpendicular (minimum T_{ion}) and parallel (maximum T_{ion}) to an imposed offset. To assess the sampling of the imposed asymmetry for each shot, the standard deviation of the offset projection in each detector LOS has been calculated. If this value is comparable for all shots, then the inferred standard deviation for the detectors should also be expected to be comparable. The standard deviation of offset projections in the nTOF LOSs is 4.5 μm for symmetric reference shot 87044 and 12.7 μm, 14.9 μm, 11.6 μm, and 13.8 μm for offset shots 87045, 87046, 87048, and 87049, respectively. The small differences between the offset shot numbers demonstrate that the standard deviation in T_{ion} can be compared between these shots; not surprisingly, the standard deviation is expected to be significantly lower for the symmetric reference shot. While the standard deviation is the lowest for 87048, even lower than for nominally centered shot 87044, 87048 does show a significantly higher average T_{ion} than 87044, indicating that significant flows are still present in this implosion although the directionality is lost. This suggests that the stalk at 42° to the offset is causing turbulent flows to be generated.

Looking at the Chimera-measurement comparison for all detectors, it is clear that some detectors measure systematically lower T_{ion} than other detectors; this is believed to be due to calibration uncertainty. Note also that variations in offset in the 10.4 m PD040 LOS are small, consistent with small T_{ion} variations [Fig. 5(e)].

The Petal-measured DT T_{ion} is contrasted to xRAGE-simulated T_{ion} in Fig. 6. Looking at the xRAGE-simulated nTOF T_{ion} for each shot (red crosses), the observed effect with lower T_{ion} for the shot with the offset away from than for the shot with the offset toward the stalk is not reproduced. However, interestingly, xRAGE also predicts a 0.33 keV higher baseline (no-flow) T_{ion} for 87045 with the offset away from than for 87049 with the offset toward the stalk (black triangles). Thus, in the simulation, a significantly larger flow enhancement is in fact predicted for the case with the offset toward the stalk. This appears consistent with the flow enhancement seen in the data for shot 87049. (Since thermal T_{ion} cannot be directly measured, we cannot directly
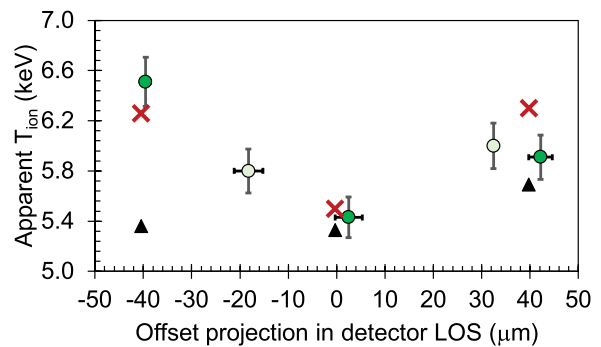

FIG. 6. Apparent T_{ion} as measured using the Petal nTOF (green circles) and simulated for the same LOS using 2D xRAGE (red crosses). Also shown is the 2D xRAGE-simulated BWTI T_{ion}, which is the thermal T_{ion} not considering the flow broadening of the neutron spectrum (black triangles).
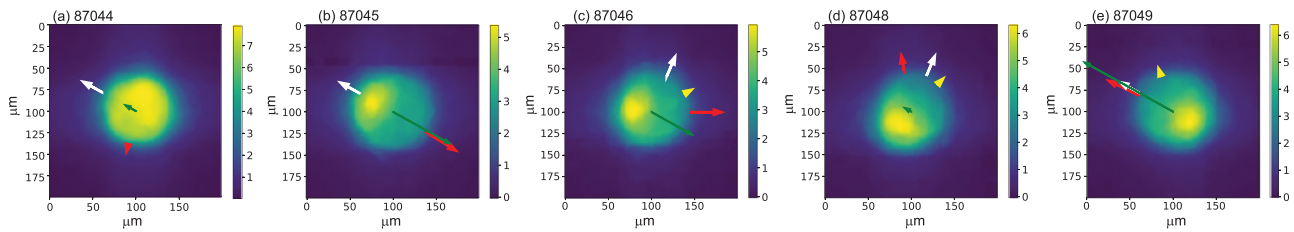
FIG. 7. Time-integrated x-ray images recorded with the GMXI diagnostic for (a) symmetric reference shot 87044, (b) shot 87045 with the offset away from the stalk, (c) shot 87046 with the offset at 76° to the stalk, (d) shot 87048 with the offset at 42° to the stalk, and (e) shot 87049 with the offset toward the stalk. The white arrow indicates the direction of the stalk mount in the GMXI plane and the red arrow the direction and magnitude of the offset. Note that there is a clear local enhancement (yellow) in the x-ray signal opposite the offset for all offset shots except 87048, where the asymmetry does not appear to correlate with the offset direction. The green arrows represent the flow velocities (direction and magnitude) as measured with the Petal nTOF (note that Petal is located in the lower right in the image–a negative measured velocity will have the arrow pointed in the opposite direction). The yellow arrows in panels (c), (d), and (e) represent the GMXI-plane projections of the mode 1 vector inferred from framing camera images.

measure flow enhancement. However, minimum T_{ion} measured for 87045 is 0.12 keV lower than for 87049, strongly suggesting that the 0.60 keV higher measured Petal T_{ion} for 87049 than for 87045 is a real flow enhancement effect.) It is interesting that the xRAGE simulation does appear to capture the higher flow with the offset toward rather than away from the stalk, even though this was not obvious from the simulated directional flow (Fig. 4).

C. Time-integrated x-ray imaging

Offsets give rise to a very clear signature in time-integrated x-ray images, arising due to higher effective drive intensity and resulting density enhancement opposite the offset (Fig. 3). GMXI-measured time-integrated x-ray images from the five implosions discussed here are shown in Fig. 7. In each image, the white arrow represents the stalk direction in the GMXI view and the red arrow the projected offset direction and magnitude in the GMXI view. The first thing to note here is that all images except the image from symmetric shot 87044 show a very clear mode 1 signature with higher x-ray intensity on one side of the implosion. It is interesting to note that this mode 1 signature appears as a local enhancement feature; the overall size of the image, inferred as the

average radius of the 30% of peak intensity contour, is very similar for all five images at 48.1 μm, 48.2 μm, 46.5 μm, 47.2 μm, and 47.3 μm for shots 87044, 87045, 87046, 87048, and 87049, respectively, and the mode content (Legendre modes 1–6) is also virtually within measurement uncertainty for this intensity contour at <5 μm for all images. The second thing to note is that this high intensity feature appears directly opposite the offset (red arrow) for all implosions except 87048. For 87048, the high-intensity feature appears to be more closely aligned with the inverse of the stalk direction (white arrow). This appears consistent with the flow and T_{ion} signatures for shot 87048 deviating from expected as discussed above: minimal flow in the offset direction was observed for 87048, and the x-ray image shows an asymmetry not aligned with the offset direction. This further supports the conclusion of unique stalk-offset interference effects with the 42° stalk-offset angle. Line-outs along the offset axis for shots 87045 and 87049 also indicate a stronger x-ray intensity asymmetry for 87049 than for 87045, supporting the conclusion from the flow/T_{ion} measurements of a larger impact on the implosion when the offset is toward rather than away from the stalk.

Also shown in Fig. 7 (green arrows) is the projection of the Petal-measured directional flow in the GMXI LOS. Note that Petal is located
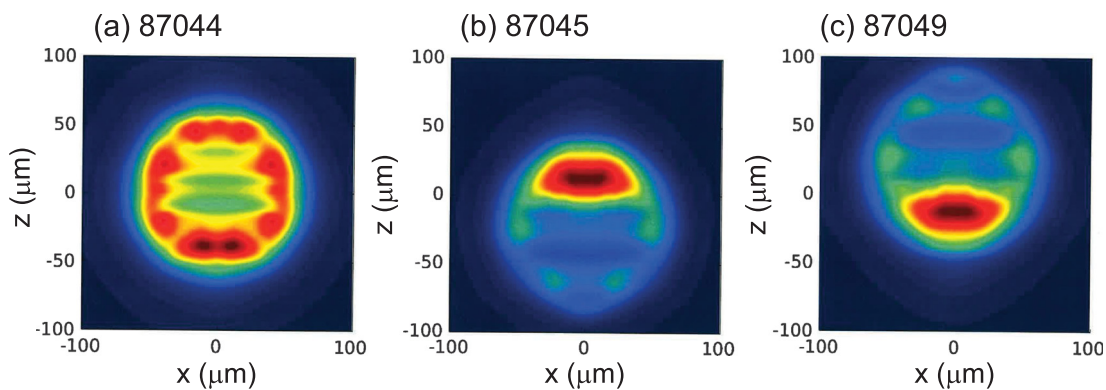

FIG. 8. 2D xRAGE-simulated time-integrated x-ray images for (a) shot 87044 (symmetric reference), (b) shot 87045 (downwards offset), and (c) shot 87049 (upwards offset). The stalk enters from the top in each image.

in the lower right in these images, meaning that an arrow toward the upper left represents a negative measured flow. The Petal-measured flows appear consistent with the GMXI-measured asymmetry.

Figure 8 shows the 2D xRAGE-simulated synthetic GMXI images. (The images have not been rotated to match the GMXI view angle–the stalk enters from the top and the offset is down for 87045 and up for 87049 in the view shown in Fig. 8.) Same as for the experimental data, the average radii inferred from these simulated images (in this case from the 40% contours) are very similar for the three cases ($60.4\,\mu m$, $66.1\,\mu m$, and $64.1\,\mu m$ for shots 87044, 87045, and 87049, respectively), and the mode content (Legendre modes 1–4) is also low ($<2.5\,\mu m$) (the slightly larger size of the simulated images may arise because the relative emissivities between bright and dark spots are different in simulation and measurement). The high-intensity features observed in the measurements for the offset shots are very clearly reproduced in the simulations. An interesting smaller x-ray intensity enhancement is also seen opposite the stalk in the simulation for centered shot 87044. This feature arises due to glue spot shadowing reducing the effective drive in the direction of the stalk, leading to a relative laser intensity enhancement opposite the stalk. This might be a

potential explanation for the smaller perturbation in the case with the offset away from rather than toward the stalk: with the offset away from the stalk, we get a relative enhancement in laser drive intensity in the direction of the stalk, which might be compensated by glue spot shadowing, with the two effects canceling each other for a more uniform implosion.

D. Time-resolved x-ray imaging

As described in Sec. II, time-resolved x-ray imaging was also fielded on these experiments in two LOSs with the goal of measuring directional capsule motion for comparison with nuclear data. Examples of measured images from $\theta = 37°$, $\phi = 162°$ for shots 87045 and 87049 are shown in Fig. 9. The first thing to note here is that the images clearly show the signature of the stalk [which enters almost perpendicular ($101°$) to the framing camera view] at the top of each image. From these images, it appears as though the capsule for 87045 with the offset away from the stalk is "taking off" from the stalk feature, while the capsule for 87049 with the offset toward the stalk is pushed closer to the stalk feature. This is another potential explanation
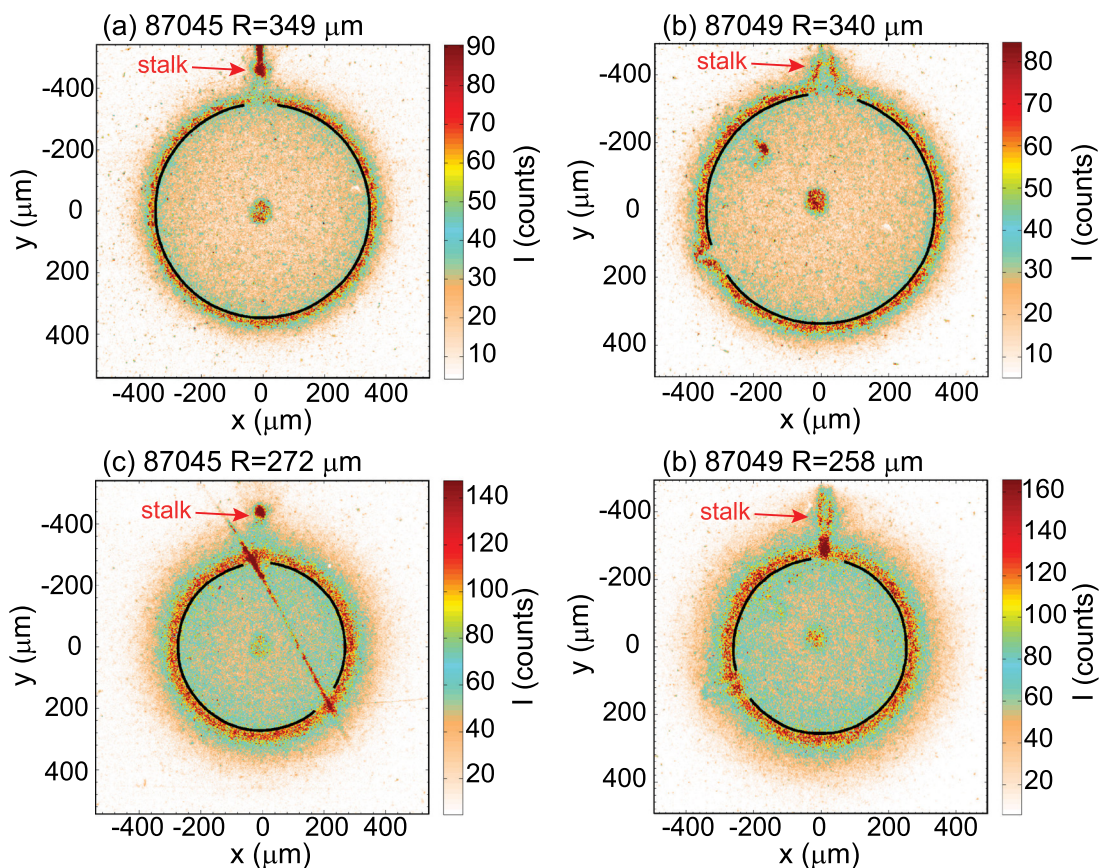

FIG. 9. Framing camera images obtained using a framing camera fielded in TIM2 with $\theta = 37°$, $\phi = 162°$ for (a) and (c) shot 87045 with the offset away from the stalk and (b) and (d) shot 87049 with the offset toward the stalk. The images in (a) and (b) are taken about 220 ps prior to the images in (c) and (d). The images visually show how the stalk perturbation is larger for the case with the offset toward (87049) rather than away from (87045) the stalk. The feature visible in the lower left corner of the images for 87049 $\sim$120° from the stalk arises due to residual glue from an initial, failed, stalk mount of this target.

TABLE VII. Mode 1 vector inferred from framing camera images at $\theta = 37°$, $\phi = 162°$ and $\theta = 101°$, $\phi = 270°$, with positions normalized to a non-imploding target (shot 87050). These data are only available for shots 87046–87049. Also shown is the angle between the framing-camera-inferred mode 1 vector and the target offset direction as measured using a high speed video (HSV) and x-ray pinhole cameras (XRPC), respectively.

Shot	Mode 1 vector inferred from SFC2 and SFC3			Angle to HSV offset (°)	Angle to XRPC offset (°)
	r (μm)	θ (°)	ϕ (°)		
87046	8.1	61.0	140.9	32.4	33.7
87048	8.7	49.8	113.6	56.1	51.0
87049	10.2	48.6	35.0	41.7	39.6

for the larger apparent perturbation in the case with the offset toward rather than away from the stalk. The second thing to note is the slight feature in the 87049 images at ∼120° counterclockwise from the stalk. This is believed to be the signature of the small residual glue spot from the capsule for 87049 falling off the stalk and having to be remounted. Fortunately, the orientation of this feature makes it unlikely to significantly impact directional flow/$T_{\rm ion}$ measurements in the Petal LOS.

In-flight mode 1 vectors inferred from the framing camera images for shots 87046, 87048, and 87049 using the method described in Ref. 54 are summarized in Table VII (unfortunately, neither framing camera obtained good data on 87044 and only one on 87045, so vectors cannot be inferred for those shots). In the analysis, the in-flight modes are interpreted to be mode 1 at convergence radius R = 200 μm. Mode 1 is assumed to grow linearly (in fact, the measured trajectory is approximately linear). r in the table should be interpreted as the distance between the initial target position and the inferred position at R = 200 μm. With R = 200 μm happening at an average time of ∼0.98 ns, this means the target motion up until this point has been ∼8–10 km/s. This is a bit lower than the velocities inferred from the nTOF measurements, which is not surprising: the velocity is likely to increase through bang time (which is ∼1.4 ns), and the velocity of the hot core is also likely to be faster than the velocity of the shell (Fig. 10). The direction of the x-ray inferred motion compares fairly well to the offset direction as can be seen in Table VII. The projection of the direction of the x-ray inferred motion in the GMXI view has also been added in Fig. 7 (yellow arrows). This again shows that the x-ray inferred directional motion aligns fairly well with the offset direction (red arrows). Uncertainties in the x-ray-inferred vectors have not been quantified, but they are expected to be relatively large due to only two views being available for these experiments.

E. Yields

A very important question is how the stalk interference impacts implosion yields. Measured, DRACO, Chimera, and xRAGE simulated yields are shown normalized to the yield for nominally centered implosion 87044 in Fig. 11(a). As can be seen, the highest yield is observed for the implosion with the offset away from the stalk, 87045. This becomes extra interesting given that yield, in the absence of stalk, is expected to scale inversely with shell thickness and positively with laser energy for these implosions, as both these factors lead to higher implosion velocity. Table I shows that shot 87045 has the highest reported shell thickness and ties for the lowest laser energy of all these shots. This is reflected in the DRACO simulations, which consequently predict the lowest yield for this shot. In contrast, the xRAGE

simulations do predict a yield enhancement for shot 87045, although not quite as high as expected from the measurements. This is especially intriguing given that thinner shells do generally lead to higher velocity and hence higher yields also in xRAGE. In the present xRAGE simulations, the peak shell kinetic energy is 12% higher for 87049 than for shot 87045 because of its thinner shell. The higher xRAGE-simulated yield for 87045 is definitely arising because of a higher simulated thermal temperature for this shot—this suggests that the asymmetries are combining to produce a more uniform compression of the gas in 87045 and hence getting a more efficient conversion of shell kinetic energy to gas internal energy. Chimera predicts lower yields for the offset implosions. As a reminder, these simulations consider neither CBET nor capsule shell thickness variations. The trend observed in Chimera yields is believed to be due to variations in absolute capsule offset magnitude (see Table II) in combination with the as-shot laser drive variations. (As discussed in Sec. III, DRACO, in contrast, predicts minimal impact of the offsets on yield; however, this lack of impact of offset on yield in the simulation has been demonstrated to be because of the inclusion of CBET.[50])
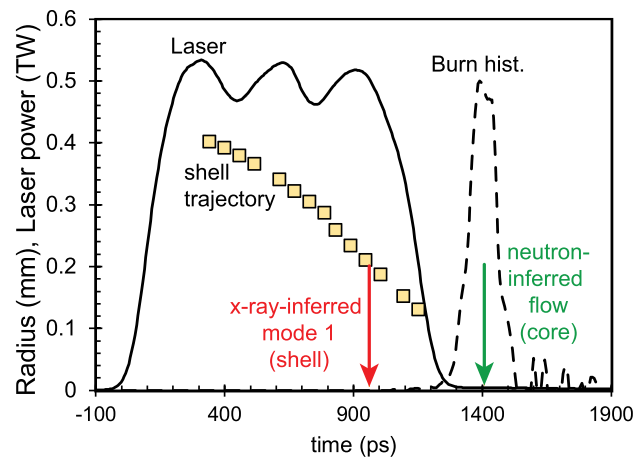

FIG. 10. Implosion laser pulse (solid black line), shell trajectory (yellow squares, measured using the framing camera at $\theta = 37°$, $\phi = 162°$), and burn history (dashed black line, measured using NTD, arbitrary units) for shot 87049. The arrows illustrate the approximate probe times for the x-ray inferred mode 2 and the neutron-inferred flow. In addition to different probe times, the two measurements also probe different parts of the implosion, with the x-ray mode 1 being inferred from the shell trajectory and the flow from the hot, central, burning fuel.

Replotting the measured yields vs offset projection in the stalk direction [Fig. 11(b)], a clear trend is seen for the offset shots with gradually increasing yields with offset further from the stalk direction (negative projection). This suggests, in agreement with flow, T_{ion}, and x-ray image observations discussed above, that the impact of the stalk mount on the implosion is highly sensitive to the stalk-offset angle. It is puzzling though that the nominally centered implosion 87044 does not follow this trend. The low observed yield on shot 87044 is not fully understood at this time, but it is interesting that xRAGE also predicts the lowest yield for this implosion. This might suggest that the impact of the stalk is partly mitigated by the offset.

V. HOW IS THE STALK PERTURBING THE IMPLOSION?

To briefly restate the conclusions from the data discussed above, directional flow, T_{ion}, time-integrated x-ray imaging measurements, and yields from these implosions all suggest a larger impact on the implosion (higher flow, lower yield, and larger asymmetry) when the offset is toward rather than away from the stalk. Flow, T_{ion}, and x-ray images also suggest smaller LOS variations in flow and less consistent asymmetry when the stalk is at 42° to the offset. Yields for the offset implosions scale with offset projection in the stalk LOS. While the

FIG. 11. (a) Measured (black circles), 2D xRAGE-simulated (red crosses), 2D DRACO-simulated (gray triangles), and 3D Chimera-simulated (gray plus signs) yields normalized to the yield for nominally centered implosion 87044 in each case. (b) Absolute measured yield plotted vs offset projection in the stalk direction, using the average projection from HSV and XRPC-measured offsets.

exact nature of the stalk perturbation cannot be inferred from these observations, two theories for what might dynamically be going on were presented in the text above: (i) when the offset is toward the stalk, then the capsule is pushed into the stalk mount, thus generating a larger perturbation, and (ii) when the offset is away from the stalk, then the drive is weaker away from the stalk due to the offset and toward the stalk due to glue spot shadowing, with the two effects compensating each other.

Some of the observed effects are reproduced in the 2D xRAGE simulations, which do consider the stalk mount, specifically the glue spot. These include a higher simulated yield for shot 87045 than for shot 87049 in spite of thicker shell and lower laser energy for shot 87045, both of which would generally be expected to lead to lower relative yield. They also include a smaller flow enhancement in T_{ion} for shot 87045 than for shot 87049. Figure 12 shows 2D xRAGE-simulated contaminant density maps. The stalk enters from the top in these images, which show how the shell and glue material are entrained into the hot spot by the jet formed due to glue spot drive shadowing. It is very interesting to study how different the jet appears depending on the direction of the offset. For shot 87045, the offset is away from the stalk (down in the image) and the contaminant jet is narrow and centralized. For shot 87049, the offset is toward the stalk (up in the image), and the contaminant jet becomes much broader, spreading along the edge of the capsule. From looking at these images, it appears as though the stalk impact would be larger for 87045. Still 87045 gives higher yield, higher T_{ion}, and smaller flow enhancement in spite of, as mentioned, the thicker shell and lower laser energy than shot 87049. This is likely because of the compensating effects of glue spot drive shadowing and offset-boosted local laser intensity in this simulation.

While they capture some of the trends seen in the data, the 2D xRAGE simulations do not fully capture all observables. Part of this could be due to the limitation of the 2D geometry. There is intrinsic as-shot drive asymmetry that is not considered in the simulations, and there is also some off-axis component to the as-shot offsets, which is not considered. Another possibility is stalk shadowing. As mentioned in Sec. III, the xRAGE simulation only includes the glue and not the stalk itself because earlier simulations showed minimal impact of the stalk due to early full ablation of the stalk material. Measurements and simulations of the fill tube used in indirect drive ICF implosions at the National Ignition Facility have demonstrated the imprint of fill tube shadowing on NIF implosions.[76] A simple static VisRad calculation including the stalk for one of the present implosions suggests that a similar effect may arise due to the stalk as well (Fig. 13). As the plasma evolves, the stalk's cross-sectional profile will expand due to blow-off, blocking more light and potentially making this effect larger.

VI. SUMMARY AND CONCLUSIONS

In this paper, we have described a set of OMEGA experiments with intentionally imposed capsule offsets at different angles to the capsule stalk mount, designed to directly test the stalk impact on these implosions. The impact of the stalk on implosion dynamics is seen in flow signatures in neutron spectra, time-integrated x-ray images, and implosion yields, with the observables seen to depend strongly on the stalk-offset angle. With the offset directly toward the stalk, a maximum
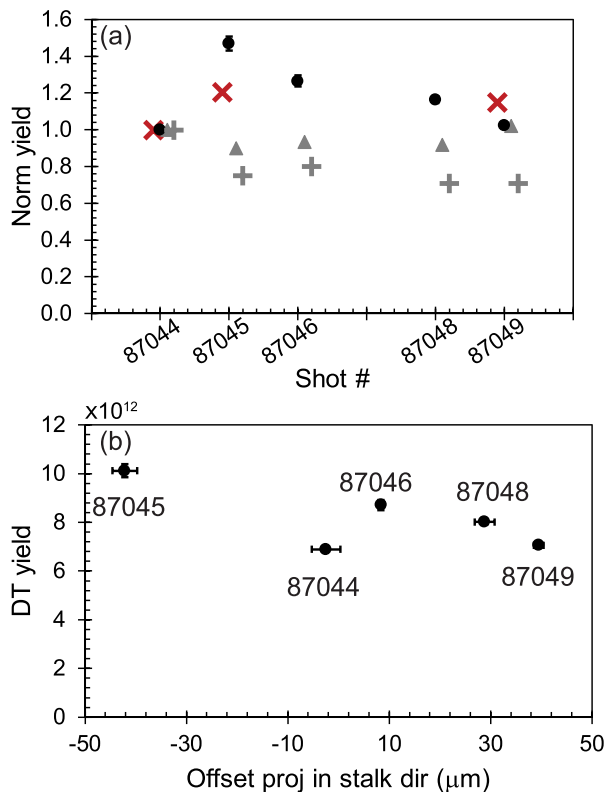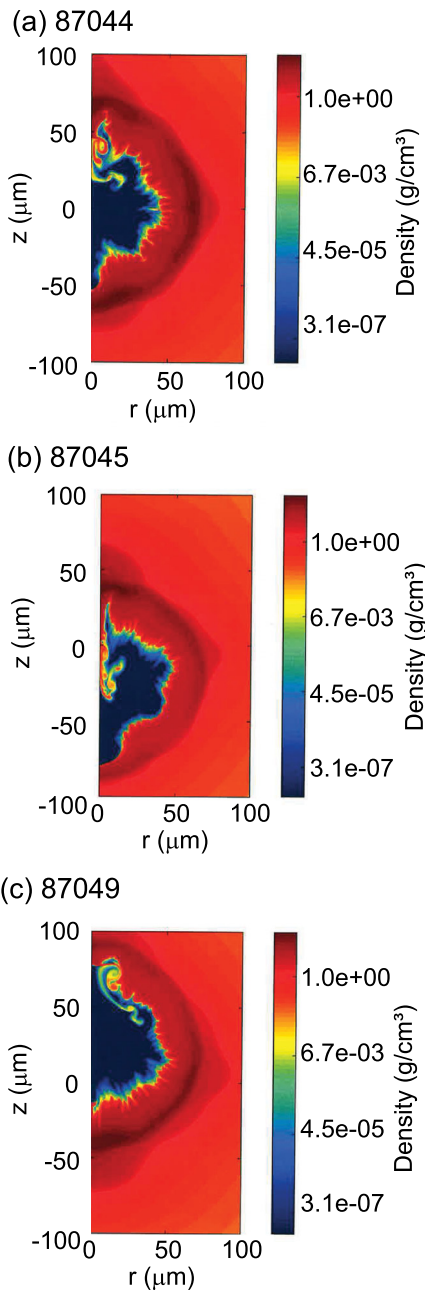
(a) 87044

(b) 87045

(c) 87049

FIG. 12. 2D xRAGE-simulated contaminant density maps for (a) shot 87044 (symmetric reference), (b) shot 87045 (downwards offset), and (c) shot 87049 (upwards offset). The stalk is entering from the top in each image. These contaminant maps clearly show how the shell/glue material is entrained into the hot spot by the jet formed due to drive shadowing.

FIG. 13. Static VisRad simulation of an on-center capsule including stalk and glue spot. There is a clear spoke pattern from stalk shadowing.

enhancement in T_{ion} are seen, along with a less consistent time-integrated x-ray image. Interestingly, in spite of the large impact of the stalk mount on the flow field for the offset implosions, no directional flow is observed for the nominally centered (stalk only) implosion.

Clear differences are seen between the data and the DRACO and Chimera simulations not considering the stalk mount, demonstrating the need to include this feature to accurately model implosion dynamics. The data presented in this paper provide an important benchmark for future simulations of the stalk mount impact on implosions. The yield trend, flow enhancement with the offset toward the stalk, and minimal directional flow with stalk only are all reproduced in the 2D xRAGE simulations, which are the only simulations brought to bear on these experiments that consider the capsule stalk mount (specifically the glue). However, these simulations do still overestimate the directional flow and total yields and predict a higher-than-observed T_{ion} for the case with the offset away from the stalk. These differences could be due to the 2D geometry of the xRAGE simulations not capturing the small as-shot drive asymmetry or the as-shot offset component perpendicular to the stalk.

While the impact of the stalk is clearly demonstrated through the results presented in this paper, further work will be required to conclusively determine the exact nature of the impact. Two possible hypotheses for how the stalk is impacting these implosions have been discussed above; both may contribute. The first has to do with glue shadowing. The offset gives rise to a laser drive asymmetry on the capsule with stronger relative drive away from the offset. This drive asymmetry is partly compensated when the offset is away from the stalk but enhanced when the offset is toward the stalk, since glue shadowing leads to locally reduced drive in the direction of the stalk. This drive compensation effect is captured in xRAGE simulations and is likely the reason why the observed difference in yield and flow with offset toward or away from the stalk are reproduced in the xRAGE simulations. The second has to do with stalk shadowing. Consistent with fill tube shadowing observations in indirect drive ICF, VisRad simulations suggest that a stalk shadowing effect with locally reduced laser drive in a spoke-pattern around the stalk may also arise in direct drive. This could potentially significantly impact the signature of the stalk mount on implosion dynamics in that it changes the asymmetry seed pattern. Further work is required to address the question of stalk shadowing and to address the relative impact of the stalk itself vs the glue. We

impact is seen, with the largest directional flow, the lowest yield, and a large asymmetry in the x-ray images. In contrast, with the offset directly away from the stalk, maximum yield, smaller directional flow, and smaller asymmetry in the x-ray images are observed. With the offset at 42° to the stalk, minimal directional flow but substantial flow
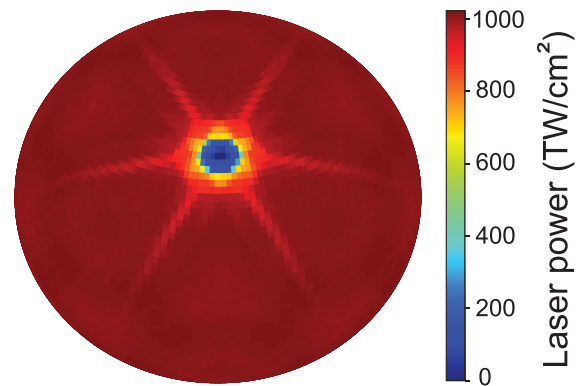
note in this context that while the results presented in this paper cannot be expected to quantitatively directly translate to other direct-drive implosion types, such as cryogenically layered implosions, or facilities, such as polar-direct drive at the National Ignition Facility,[72] either of the two mechanisms discussed for how the stalk impacts the implosions suggest that similar effects and trends as those discussed here will be at play in any direct-drive configuration involving a stalk mount.

Finally, we note that while the total impact of the stalk only on implosion performance cannot be quantified in this way since all implosions are fielded on a stalk, it is obvious from the presented data that the stalk must be considered when interpreting asymmetry signatures and when attempting to achieve high-performing, symmetrically converging implosions.

ACKNOWLEDGMENTS

APPENDIX A: ρR MEASUREMENTS

Figure 14 shows the total and shell ρR as inferred from proton spectral measurements by CPS1, CPS2, MRS, and WRFs in TIM3 and P2NDI as a function of offset projection in the detector LOS for each shot (of the five total and five shell ρR numbers shown for each shot, one is from each detector). These data suggest that the ρR asymmetry is dominated by the offset for these implosions, showing higher ρR opposite the offset, consistent with the higher density predicted in this direction (compare Fig. 3).

The large error bars in the offset projection for the shell ρR measurements reflect the broad scattering angle sampling of this measurement; proton energies $E_p > 11$ MeV are used to infer shell ρR, corresponding to a LOS cone with an opening angle 28° around each detector.
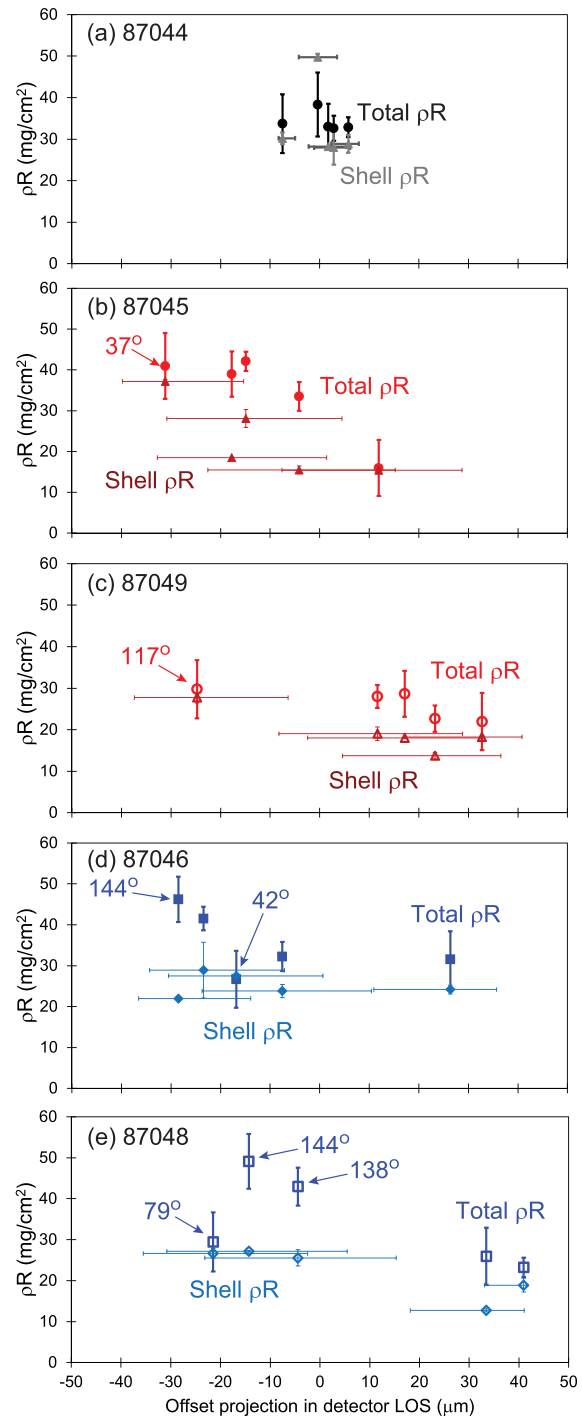
FIG. 14. Total (inferred from the D3He-p downshift) and shell (inferred from the KO-p yield) ρR for (a), (b), and (c) shots 87044, 87045, and 87049, with the capsule held by TIM4 (with circles and triangles representing total and shell ρR, respectively) and (d) and (e) shots 87046 and 87048, with the capsule held by TPS2 (with squares and diamonds representing total and shell ρR, respectively). The angles shown in the figure represent the angle to the stalk for the indicated measurements. The ρR asymmetry appears dominated by the offset.

REFERENCES

[1] J. Lindl, O. Landen, J. Edwards, and NIC Team, Phys. Plasmas **21**, 020501 (2014).

[2] R. S. Craxton, K. S. Anderson, T. R. Boehly, V. N. Goncharov, D. R. Harding, J. P. Knauer, R. L. McCrory, P. W. McKenty, D. D. Meyerhofer, J. F. Myatt, A. J. Schmitt, J. D. Sethian, R. W. Short, S. Skupsky, W. Theobald, W. L. Kruer, K. Tanaka, R. Betti, T. J. B. Collins, J. A. Delettrez, S. X. Hu, J. A. Marozas, A. V. Maximov, D. T. Michel, P. B. Radha, S. P. Regan, T. C. Sangster, W. Seka, A. A. Solodov, J. M. Soures, C. Stoeckl, and J. D. Zuegel, Phys. Plasmas **22**, 110501 (2015).

[3] S. Atzeni and J. Meyer-Ter-Vehn, *The Physics of Inertial Fusion* (Oxford University Press, 2004).

[4] O. A. Hurricane, D. A. Callahan, D. T. Casey, E. L. Dewald, T. R. Dittrich, T. Döppner, S. Haan, D. E. Hinkel, L. F. Berzak Hopkins, O. Jones, A. L. Kritcher, S. Le Pape, T. Ma, A. G. MacPhee, J. L. Milovich, J. Moody, A. Pak, H.-S. Park, P. K. Patel, J. E. Ralph, H. F. Robey, J. S. Ross, J. D. Salmonson, B. K. Spears, P. T. Springer, R. Tommasini, F. Albert, L. R. Benedetti, R. Bionta, E. Bond, D. K. Bradley, J. Caggiano, P. M. Celliers, C. Cerjan, J. A. Church, R. Dylla-Spears, D. Edgell, M. J. Edwards, D. Fittinghoff, M. A. Barrios Garcia, A. Hamza, R. Hatarik, H. Herrmann, M. Hohenberger, D. Hoover, J. L. Kline, G. Kyrala, B. Kozioziemski, G. Grim, J. E. Field, J. Frenje, N. Izumi, M. Gatu Johnson, S. F. Khan, J. Knauer, T. Kohut, O. Landen, F. Merrill, P. Michel, S. R. Nagel, A. Nikroo, T. Parham, R. R. Rygg, D. Sayre, M. Schneider, D. Shaughnessy, D. Strozzi, R. P. J. Town, D. Turnbull, P. Volegov, A. Wan, K. Widmann, C. Wilde, and C. Yeamans, Nat. Phys. **12**, 800 (2016).

[5] S. LePape, L. F. Berzak Hopkins, L. Divol, A. Pak, E. L. Dewald, S. Bhandarkar, L. R. Bennedetti, T. Bunn, J. Biener, J. Crippen, D. Casey, D. Edgell, D. N. Fittinghoff, M. Gatu-Johnson, C. Goyon, S. Haan, R. Hatarik, M. Havre, D. D.-M. Ho, N. Izumi, J. Jaquez, S. F. Khan, G. A. Kyrala, T. Ma, A. J. Mackinnon, A. G. MacPhee, B. J. MacGowan, N. B. Meezan, J. Milovich, M. Millot, P. Michel, S. R. Nagel, A. Nikroo, P. Patel, J. Ralph, J. S. Ross, N. G. Rice, D. Strozzi, M. Stadermann, P. Volegov, C. Yeamans, C. Weber, C. Wild, D. Callahan, and O. A. Hurricane, Phys. Rev. Lett. **120**, 245003 (2018).

[6] S. P. Regan, V. N. Goncharov, I. V. Igumenshchev, T. C. Sangster, R. Betti, A. Bose, T. R. Boehly, M. J. Bonino, E. M. Campbell, D. Cao, T. J. B. Collins, R. S. Craxton, A. K. Davis, J. A. Delettrez, D. H. Edgell, R. Epstein, C. J. Forrest, J. A. Frenje, D. H. Froula, M. Gatu Johnson, V. Yu. Glebov, D. R. Harding, M. Hohenberger, S. X. Hu, D. Jacobs-Perkins, R. Janezic, M. Karasik, R. L. Keck, J. H. Kelly, T. J. Kessler, J. P. Knauer, T. Z. Kosc, S. J. Loucks, J. A. Marozas, F. J. Marshall, R. L. McCrory, P. W. McKenty, D. D. Meyerhofer, D. T. Michel, J. F. Myatt, S. P. Obenschain, R. D. Petrasso, P. B. Radha, B. Rice, M. J. Rosenberg, A. J. Schmitt, M. J. Schmitt, W. Seka, W. T. Shmayda, M. J. Shoup III, A. Shvydky, S. Skupsky, A. A. Solodov, C. Stoeckl, W. Theobald, J. Ulreich, M. D. Wittman, K. M. Woo, B. Yaakobi, and J. D. Zuegel, Phys. Rev. Lett. **117**, 025001 (2016).

[7] R. H. H. Scott, D. S. Clark, D. K. Bradley, D. A. Callahan, M. J. Edwards, S. W. Haan, O. S. Jones, B. K. Spears, M. M. Marinak, R. P. J. Town, P. A. Norreys, and L. J. Suter, Phys. Rev. Lett. **110**, 075001 (2013).

[8] B. K. Spears, M. J. Edwards, S. Hatchett, J. Kilkenny, J. Knauer, A. Kritcher, J. Lindl, D. Munro, P. Patel, H. F. Robey, and R. P. J. Town, Phys. Plasmas **21**, 042702 (2014).

[9] A. L. Kritcher, R. Town, D. Bradley, D. Clark, B. Spears, O. Jones, S. Haan, P. T. Springer, J. Lindl, R. H. H. Scott, D. Callahan, M. J. Edwards, and O. L. Landen, Phys. Plasmas **21**, 042708 (2014).

[10] A. L. Kritcher, D. E. Hinkel, D. A. Callahan, O. A. Hurricane, D. Clark, D. T. Casey, E. L. Dewald, T. R. Dittrich, T. Döppner, M. A. Barrios Garcia, S. Haan, L. F. Berzak Hopkins, O. Jones, O. Landen, T. Ma, N. Meezan, J. L. Milovich, A. E. Pak, H.-S. Park, P. K. Patel, J. Ralph, H. F. Robey, J. D. Salmonson, S. Sepke, B. Spears, P. T. Springer, C. A. Thomas, R. Town, P. M. Celliers, and M. J. Edwards, Phys. Plasmas **23**, 052709 (2016).

[11] I. V. Igumenshchev, V. N. Goncharov, F. J. Marshall, J. P. Knauer, E. M. Campbell, C. J. Forrest, D. H. Froula, V. Y. Glebov, R. L. McCrory, S. P. Regan, T. C. Sangster, S. Skupsky, and C. Stoeckl, Phys. Plasmas **23**, 052702 (2016).

[12] I. V. Igumenshchev, D. T. Michel, R. C. Shah, E. M. Campbell, R. Epstein, C. J. Forrest, V. Yu. Glebov, V. N. Goncharov, J. P. Knauer, F. J. Marshall, R. L. McCrory, S. P. Regan, T. C. Sangster, C. Stoeckl, A. J. Schmitt, and S. Obenschein, Phys. Plasmas **24**, 056307 (2017).

[13] R. C. Shah, B. M. Haines, F. J. Wysocki, J. F. Benage, J. A. Fooks, V. Glebov, P. Hakel, M. Hoppe, I. V. Igumenshchev, G. Kagan, R. C. Mancini, F. J. Marshall, D. T. Michel, T. J. Murphy, M. E. Schoff, K. Silverstein, C. Stoeckl, and B. Yaakobi, Phys. Rev. Lett. **118**, 135001 (2017).

[14] A. Bose, R. Betti, D. Shvarts, and K. M. Woo, Phys. Plasmas **24**, 102704 (2017).

[15] M. Gatu Johnson, B. D. Appelbe, J. P. Chittenden, J. Delettrez, C. Forrest, J. A. Frenje, V. Y. Glebov, W. Grimble, B. M. Haines, I. Igumenshchev, R. Janezic, J. P. Knauer, B. Lahmann, F. J. Marshall, T. Michel, F. H. Séguin, C. Stoeckl, C. Walsh, A. B. Zylstra, and R. D. Petrasso, Phys. Rev. E **98**, 051201(R) (2018).

[16] K. M. Woo, R. Betti, D. Shvarts, A. Bose, D. Patel, R. Yan, P.-Y. Chang, O. M. Mannion, R. Epstein, J. A. Delettrez, M. Charissis, K. S. Anderson, P. B. Radha, A. Shvydky, I. V. Igumenshchev, V. Gopalaswamy, A. R. Christopherson, J. Sanz, and H. Aluie, Phys. Plasmas **25**, 052704 (2018).

[17] A. Bose, R. Betti, D. Mangino, K. M. Woo, D. Patel, A. R. Christopherson, V. Gopalaswamy, O. M. Mannion, S. P. Regan, V. N. Goncharov, D. H. Edgell, C. J. Forrest, J. A. Frenje, M. Gatu Johnson, V. Y. Glebov, I. V. Igumenshchev, J. P. Knauer, F. J. Marshall, P. B. Radha, R. Shah, C. Stoeckl, W. Theobald, T. C. Sangster, D. Shvarts, and E. M. Campbell, Phys. Plasmas **25**, 062701 (2018).

[18] K. M. Woo, R. Betti, D. Shvarts, O. M. Mannion, D. Patel, V. N. Goncharov, K. S. Anderson, P. B. Radha, J. P. Knauer, A. Bose, V. Gopalaswamy, A. R. Christopherson, E. M. Campbell, J. Sanz, and H. Aluie, Phys. Plasmas **25**, 102710 (2018).

[19] P. T. Springer, O. A. Hurricane, J. H. Hammer, R. Betti, D. A. Callahan, E. M. Campbell, D. T. Casey, C. J. Cerjan, D. Cao, E. Dewald, L. Divol, T. Doeppner, M. J. Edwards, J. E. Field, C. Forrest, J. Frenje, J. A. Gaffney, M. Gatu-Johnson, V. Glebov, V. N. Goncharov, G. P. Grim, E. Hartouni, R. Hatarik, D. E. Hinkel, L. F. B. Hopkins, I. Igumenshchev, P. Knapp, J. P. Knauer, A. L. Kritcher, O. Landen, A. Pak, S. Le Pape, T. Ma, A. G. MacPhee, D. H. Munro, R. C. Nora, P. K. Patel, L. Peterson, P. B. Radha, S. P. Regan, H. Rinderknecht, C. Sangster, B. K. Spears, and C. Stoeckl, Nucl. Fusion **59**, 032009 (2019).

[20] M. Gatu Johnson, B. D. Appelbe, J. P. Chittenden, A. Crilly, J. Delettrez, C. Forrest, J. A. Frenje, V. Y.Glebov, W. Grimble, B. M. Haines, I. Igumenshchev, R. Janezic, J. P. Knauer, B. Lahmann, F. J. Marshall, T. Michel, F. H. Séguin, C. Stoeckl, C. Walsh, A. B. Zylstra, and R. D. Petrasso, Phys. Plasmas **26**, 012706 (2019).

[21] I. V. Igumenshchev, F. J. Marshall, J. A. Marozas, V. A. Smalyuk, R. Epstein, V. N. Goncharov, T. J. B. Collins, T. C. Sangster, and S. Skupsky, Phys. Plasmas **16**, 082701 (2009).

[22] B. M. Haines, G. P. Grim, J. R. Fincke, R. C. Shah, C. J. Forrest, K. Silverstein, F. J. Marshall, M. Boswell, M. M. Fowler, R. A. Gore, A. C. Hayes-Sterbenz, G. Jungman, A. Klein, R. S. Rundberg, M. J. Steinkamp, and J. B. Wilhelmy, Phys. Plasmas **23**, 072709 (2016).

[23] C. Stoeckl, R. Epstein, R. Betti, W. Bittle, J. A. Delettrez, C. J. Forrest, V. Yu. Glebov, V. N. Goncharov, D. R. Harding, I. V. Igumenshchev, D. W. Jacobs-Perkins, R. T. Janezic, J. H. Kelly, T. Z. Kosc, R. L. McCrory, D. T. Michel, C. Mileham, P. W. McKenty, F. J. Marshall, S. F. B. Morse, S. P. Regan, P. B. Radha, B. Rice, T. C. Sangster, M. J. ShoupIII, W. T. Shmayda, S. Sorce, W. Theobald, J. Ulreich, M. D. Wittman, D. D. Meyerhofer, J. A. Frenje, M. Gatu Johnson, and R. D. Petrasso, Phys. Plasmas **24**, 056304 (2017).

[24] R. Tommasini, J. E. Field, B. A. Hammel, O. L. Landen, S. W. Haan, C. Aracne-Ruddle, L. R. Benedetti, D. K. Bradley, D. A. Callahan, E. L. Dewald, T. Doeppner, M. J. Edwards, O. A. Hurricane, N. Izumi, O. A. Jones, T. Ma, N. B. Meezan, S. R. Nagel, J. R. Rygg, K. S. Segraves, M. Stadermann, R. J. Strauser, and R. P. J. Town, Phys. Plasmas **22**, 056315 (2015).

[25] C. R. Weber, D. T. Casey, D. S. Clark, B. A. Hammel, A. MacPhee, J. Milovich, D. Martinez, H. F. Robey, V. A. Smalyuk, M. Stadermann, P. Amendt, S. Bhandarkar, B. Chang, C. Choate, J. Crippen, S. J. Felker, J. E. Field, S. W. Haan, S. Johnson, J. J. Kroll, O. L. Landen, M. Marinak, M. Mcinnis, A. Nikroo, N. Rice, and S. M. Sepke, Phys. Plasmas **24**, 056302 (2017).

[26] J. R. Rygg, J. A. Frenje, C. K. Li, F. H. Séguin, R. D. Petrasso, F. J. Marshall, J. A. Delettrez, J. P. Knauer, D. D. Meyerhofer, and C. Stoeckl, Phys. Plasmas **15**, 034505 (2008).

[27] A. Pak, L. Divol, A. L. Kritcher, T. Ma, J. E. Ralph, B. Bachmann, L. R. Benedetti, D. T. Casey, P. M. Celliers, E. L. Dewald, T. Döppner, J. E. Field, D. E. Fratanduono, L. F. Berzak Hopkins, N. Izumi, S. F. Khan, O. L. Landen, G.

A. Kyrala, S. LePape, M. Millot, J. L. Milovich, A. S. Moore, S. R. Nagel, H.-S. Park, J. R. Rygg, D. K. Bradley, D. A. Callahan, D. E. Hinkel, W. W. Hsing, O. A. Hurricane, N. B. Meezan, J. D. Moody, P. Patel, H. F. Robey, M. B. Schneider, R. P. J. Town, and M. J. Edwards, Phys. Plasmas **24**, 056306 (2017).

[28]L. Divol, A. Pak, L. F. Berzak Hopkins, S. L. Pape, N. B. Meezan, E. L. Dewald, D. D.-M. Ho, S. F. Khan, A. J. Mackinnon, J. S. Ross, D. P. Turnbull, C. Weber, P. M. Celliers, M. Millot, L. R. Benedetti, J. E. Field, N. Izumi, G. A. Kyrala, T. Ma, S. R. Nagel, J. R. Rygg, D. Edgell, A. G. Macphee, C. Goyon, M. Hohenberger, B. J. MacGowan, P. Michel, D. Strozzi, W. Cassata, D. Casey, D. N. Fittinghoff, N. Gharibyan, R. Hatarik, D. Sayre, P. Volegov, C. Yeamans, B. Bachmann, T. Döppner, J. Biener, J. Crippen, C. Choate, H. Huang, C. Kong, A. Nikroo, N. G. Rice, M. Stadermann, S. D. Bhandarkar, S. Haan, B. Kozioziemski, W. W. Hsing, O. L. Landen, J. D. Moody, R. P. J. Town, D. A. Callahan, O. A. Hurricane, and M. J. Edwards, Phys. Plasmas **24**, 056309 (2017).

[29]T. R. Boehly, D. L. Brown, R. S. Craxton, R. L. Keck, J. P. Knauer, J. H. Kelly, T. J. Kessler, S. A. Kumpan, S. J. Loucks, S. A. Letzring, F. J. Marshall, R. L. McCrory, S. F. B. Morse, W. Seka, J. M. Soures, and C. P. Verdon, Opt. Commun. **133**, 495 (1997).

[30]V. Gopalaswamy, R. Betti, J. P. Knauer, N. Luciani, D. Patel, K. M. Woo, A. Bose, I. V. Igumenshchev, E. M. Campbell, K. S. Anderson, K. A. Bauer, M. J. Bonino, D. Cao, A. R. Christopherson, G. W. Collins, T. J. B. Collins, J. R. Davies, J. A. Delettrez, D. H. Edgell, R. Epstein, C. J. Forrest, D. H. Froula, V. Y. Glebov, V. N. Goncharov, D. R. Harding, S. X. Hu, D. W. Jacobs-Perkins, R. T. Janezic, J. H. Kelly, O. M. Mannion, A. Maximov, F. J. Marshall, D. T. Michel, S. Miller, S. F. B. Morse, J. Palastro, J. Peebles, P. B. Radha, S. P. Regan, S. Sampat, T. C. Sangster, A. B. Sefkow, W. Seka, R. C. Shah, W. T. Shmyada, A. Shvydky, C. Stoeckl, A. Solodov, W. Theobald, J. D. Zuegel, M. Gatu Johnson, R. D. Petrasso, C. K. Li, and J. A. Frenje, Nature **565**, 581 (2019).

[31]M. Gatu Johnson, D. T. Casey, J. A. Frenje, C.-K. Li, F. H. Séguin, R. D. Petrasso, R. Ashabranner, R. Bionta, S. LePape, M. McKernan, A. Mackinnon, J. D. Kilkenny, J. Knauer, and T. C. Sangster, Phys. Plasmas **20**, 042707 (2013).

[32]J. D. Kilkenny, J. A. Caggiano, R. Hatarik, J. P. Knauer, D. B. Sayre, B. K. Spears, S. V. Weber, C. B. Yeamans, C. J. Cerjan, L. Divol, M. J. Eckart, V. Yu. Glebov, H. W. Herrmann, S. LePape, D. H. Munro, G. P. Grim, O. S. Jones, L. Berzak-Hopkins, M. Gatu-Johnson, A. J. Mackinnon, N. B. Meezan, D. T. Casey, J. A. Frenje, J. M. MacNaney, R. Petrasso, H. Rinderknecht, W. Stoeffl, and A. B. Zylstra, J. Phys.: Conf. Ser. **688**, 012048 (2016).

[33]O. M. Mannion, V. Yu. Glebov, C. J. Forrest, J. P. Knauer, V. N. Goncharov, S. P. Regan, T. C. Sangster, C. Stoeckl, and M. Gatu Johnson, Rev. Sci. Instrum. **89**, 10I131 (2018).

[34]T. J. Murphy, Phys. Plasmas **21**, 072701 (2014).

[35]M. Gatu Johnson, J. P. Knauer, C. J. Cerjan, M. J. Eckart, G. P. Grim, E. P. Hartouni, R. Hatarik, J. D. Kilkenny, D. H. Munro, D. B. Sayre, B. K. Spears, R. M. Bionta, E. J. Bond, J. A. Caggiano, D. Callahan, D. T. Casey, T. Döppner, J. A. Frenje, V. Y.Glebov, O. Hurricane, A. Kritcher, S. LePape, T. Ma, A. Mackinnon, N. Meezan, P. Patel, R. D. Petrasso, J. E. Ralph, P. T. Springer, and C. B. Yeamans, Phys. Rev. E **94**, 021202(R) (2016).

[36]L. Ballabio, J. Källne, and G. Gorini, Nucl. Fusion **38**, 1723 (1998).

[37]B. Appelbe and J. Chittenden, Plasma Phys. Controlled Fusion **53**, 045002 (2011).

[38]B. J. Albright, K. Molvig, C.-K. Huang, A. N. Simakov, E. S. Dodd, N. M. Hoffman, G. Kagan, and P. F. Schmit, Phys. Plasmas **20**, 122705 (2013).

[39]G. Kagan, D. Svyatskiy, H. G. Rinderknecht, M. J. Rosenberg, A. B. Zylstra, C.-K. Huang, and C. J. McDevitt, Phys. Rev. Lett. **115**, 105002 (2015).

[40]V. Yu. Glebov, T. C. Sangster, C. Stoeckl, J. P. Knauer, W. Theobald, K. L. Marshall, M. J. Shoup III, T. Buczek, M. Cruz, T. Duffy, M. Romanofsky, M. Fox, A. Pruyne, M. J. Moran, R. A. Lerche, J. McNaney, J. D. Kilkenny, M. J. Eckart, D. Schneider, D. Munro, W. Stoeffl, R. Zacharias, J. J. Haslam, T. Clancy, M. Yeoman, D. Warwas, C. J. Horsfield, J.-L. Bourgade, O. Landoas, L. Disdier, G. A. Chandler, and R. J. Leeper, Rev. Sci. Instrum. **81**, 10D325 (2010).

[41]See http://www.lle.rochester.edu/media/about/documents/UsersGuide/05_UsersGuide.pdf for "Laboratory for Laser Energetics, National Laser Users' Facility Users Guide, University of Rochester," 2014.

[42]V. Y. Glebov, "Six DT nTOF detectors on OMEGA," in nTOF Diagnostic Workshop, LLNL, July 18 2017.

[43]W. Grimble, F. J. Marshall, and E. Lambrides, Phys. Plasmas **25**, 072702 (2018).

[44]F. J. Marshall, J. A. Delettrez, R. Epstein, R. Forties, R. L. Keck, J. H. Kelly, P. W. McKenty, S. P. Regan, and L. J. Waxer, Phys. Plasmas **11**, 251 (2004).

[45]S. Skupsky, R. W. Short, T. Kessler, R. S. Craxton, S. Letzring, and J. M. Soures, J. Appl. Phys. **66**, 3456 (1989); S. P. Regan, J. A. Marozas, R. Stephen Craxton, J. H. Kelly, W. R. Donaldson, P. A. Jaanimagi, D. Jacobs-Perkins, R. L. Keck, T. J. Kessler, D. D. Meyerhofer, T. Craig Sangster, W. Seka, V. A. Smalyuk, S. Skupsky, and J. D. Zuegel, J. Opt. Soc. Am. B **22**, 998 (2005).

[46]T. R. Boehly, V. A. Smalyuk, D. D. Meyerhofer, J. P. Knauer, D. K. Bradley, R. S. Craxton, M. J. Guardalben, S. Skupsky, and T. J. Kessler, J. Appl. Phys. **85**, 3444 (1999).

[47]See http://www.lle.rochester.edu/media/omega_facility/documentation/documents/nluf_users_guide.pdf for "Laboratory for Laser Energetics, National Laser Users' Facility Users Guide, University of Rochester," 2007.

[48]W. R. Donaldson, J. Katz, R. Huff, E. M. Hill, J. H. Kelly, J. Kwiatkowski, R. B. Brannon, and R. Boni, Rev. Sci. Instrum. **87**, 053511 (2016).

[49]J. J. MacFarlane, J. Quant. Spectrosc. Radiat. Transfer **81**, 287 (2003).

[50]K. S. Anderson, C. J. Forrest, O. M. Mannion, F. J. Marshall, R. C. Shah, J. A. Marozas, P. B. Radha, D. Edgell, R. Epstein, V. N. Goncharov, J. P. Knauer, D. T. Michel, M. Gatu Johnson, and S. Laffite, "Effect of cross-beam energy transfer on target offset asymmetry in directly-driven inertial confinement fusion implosions," Phys. Plasmas (to be published).

[51]OMEGA has recently implemented the capability to measure directional flow in four LOS, allowing reconstruction of a full velocity vector [see O. M. Mannion, J. P. Knauer, V. Y. Glebov, C. J. Forrest, A. Lui, Z. L. Mohamed, M. H. Romanofsky, C. Stoeckl, T. C. Sangster, and S. P. Regan, "A suite of neutron time-of-flight detectors to measure hot-spot motion in direct-drive inertial confinement fusion experiments on OMEGA," Nucl. Instrum. Methods Phys. Res., Sect. A (2020)]. This capability was not yet available when the experiments described here were performed.

[52]C. J. Forrest, V. Y. Glebov, V. N. Goncharov, J. P. Knauer, P. B. Radha, S. P. Regan, M. H. Romanofsky, T. C. Sangster, M. J. Shoup III, and C. Stoeckl, Rev. Sci. Instrum. **87**, 11D814 (2016).

[53]F. J. Marshall and J. A. Oertel, Rev. Sci. Instrum. **68**, 735 (1997).

[54]D. T. Michel, I. V. Igumenshchev, A. K. Davis, D. H. Edgell, D. H. Froula, D. W. Jacobs-Perkins, V. N. Goncharov, S. P. Regan, A. Shvydky, and E. M. Campbell, Phys. Rev. Lett. **120**, 125001 (2018).

[55]D. T. Casey, J. A. Frenje, M. Gatu Johnson, F. H. Séguin, C. K. Li, R. D. Petrasso, V. Y. Glebov, J. Katz, J. Magoon, D. D. Meyerhofer, T. C. Sangster, M. Shoup, J. Ulreich, R. C. Ashabranner, R. M. Bionta, A. C. Carpenter, B. Felker, H. Y. Khater, S. LePape, A. MacKinnon, M. A. Mckernan, M. Moran, J. R. Rygg, M. F. Yeoman, R. Zacharias, R. J. Leeper, K. Fletcher, M. Farrell, D. Jasion, J. Kilkenny, and R. Paguio, Rev. Sci. Instrum. **84**, 043506 (2013).

[56]D. Hicks, "Charged-particle spectroscopy: A new window on inertial confinement fusion," Ph.D. thesis (Massachusetts Institute of Technology, 1999).

[57]F. H. Séguin, J. A. Frenje, C. K. Li, D. G. Hicks, S. Kurebayashi, J. R. Rygg, B.-E. Schwartz, R. D. Petrasso, S. Roberts, J. M. Soures, D. D. Meyerhofer, T. C. Sangster, J. P. Knauer, C. Sorce, V. Y. Glebov, C. Stoeckl, T. W. Phillips, R. J. Leeper, K. Fletcher, and S. Padalino, Rev. Sci. Instrum. **74**, 975 (2003).

[58]C. K. Li, F. H. Séguin, D. G. Hicks, J. A. Frenje, K. M. Green, S. Kurebayashi, R. D. Petrasso, D. D. Meyerhofer, J. M. Soures, V. Y. Glebov, R. L. Keck, P. B. Radha, S. Roberts, W. Seka, S. Skupsky, and C. Stoeckl, Phys. Plasmas **8**, 4902 (2001).

[59]F. H. Séguin, C. K. Li, J. A. Frenje, S. Kurebayashi, R. D. Petrasso, F. J. Marshall, D. D. Meyerhofer, J. M. Soures, T. C. Sangster, C. Stoeckl, J. A. Delettrez, P. B. Radha, V. A. Smalyuk, and S. Roberts, Phys. Plasmas **9**, 3558 (2002).

[60]C. Stoeckl, R. Boni, F. Ehrne, C. J. Forrest, V. Y. Glebov, J. Katz, D. J. Lonobile, J. Magoon, S. P. Regan, M. J. Shoup III, A. Sorce, C. Sorce, T. C. Sangster, and D. Weiner, Rev. Sci. Instrum. **87**, 053501 (2016).

[61]H.-S. Bosch and G. M. Hale, Nucl. Fusion **32**, 611 (1992).

[62]W. Seka, H. A. Baldis, J. Fuchs, S. P. Regan, D. D. Meyerhofer, C. Stoeckl, B. Yaakobi, R. S. Craxton, and R. W. Short, Phys. Rev. Lett. **89**, 175002 (2002).

[63]J. Delettrez, R. Epstein, M. C. Richardson, P. A. Jaanimagi, and B. L. Henke, Phys. Rev. A **36**, 3926 (1987).

[64] P. B. Radha, V. N. Goncharov, T. J. B. Collins, J. A. Delettrez, Y. Elbaz, V. Y. Glebov, R. L. Keck, D. E. Keller, J. P. Knauer, J. A. Marozas, F. J. Marshall, P. W. McKenty, D. D. Meyerhofer, S. P. Regan, T. C. Sangster, D. Shvarts, S. Skupsky, Y. Srebro, R. P. J. Town, and C. Stoeckl, Phys. Plasmas **12**, 032702 (2005).

[65] M. Gittings, R. Weaver, M. Clover, T. Betlach, N. Byrne, R. Coker, E. Dendy, R. Hueckstaedt, K. New, W. R. Oakes, D. Ranta, and R. Stefan, Comput. Sci. Discovery **1**, 015005 (2008).

[66] B. M. Haines, C. H. Aldrich, J. M. Campbell, R. M. Rauenzahn, and C. A. Wingate, Phys. Plasmas **24**, 052701 (2017).

[67] J. P. Chittenden, B. D. Appelbe, F. Manke, K. McGlinchey, and N. P. L. Niasse, Phys. Plasmas **23**, 052708 (2016).

[68] J. T. Larsen and S. M. Lane, J. Quant. Spectrosc. Radiat. Transfer **51**, 179 (1994).

[69] J. A. Marozas, M. Hohenberger, M. J. Rosenberg, D. Turnbull, T. J. B. Collins, P. B. Radha, P. W. McKenty, J. D. Zuegel, F. J. Marshall, S. P. Regan, T. C. Sangster, W. Seka, E. M. Campbell, V. N. Goncharov, M. W. Bowers, J.-M. G. Di Nicola, G. Erbert, B. J. MacGowan, L. J. Pelz, and S. T. Yang, Phys. Rev. Lett. **120**, 085001 (2018).

[70] D. Cao, J. Moses, and J. Delettrez, Phys. Plasmas **22**, 082308 (2015).

[71] F. Weilacher, P. B. Radha, and C. J. Forrest, Phys. Plasmas **25**, 042704 (2018).

[72] P. B. Radha, M. Hohenberger, D. H. Edgell, J. A. Marozas, F. J. Marshall, D. T. Michel, M. J. Rosenberg, W. Seka, A. Shvydky, T. R. Boehly, T. J. B. Collins, E. M. Campbell, R. S. Craxton, J. A. Delettrez, S. N. Dixit, J. A. Frenje, D. H. Froula, V. N. Goncharov, S. X. Hu, J. P. Knauer, R. L. McCrory, P. W. McKenty, D. D. Meyerhofer, J. Moody, J. F. Myatt, R. D. Petrasso, S. P. Regan, T. C. Sangster, H. Sio, S. Skupsky, and A. Zylstra, Phys. Plasmas **23**, 056305 (2016).

[73] J. A. Marozas, M. Hohenberger, M. J. Rosenberg, D. Turnbull, T. J. B. Collins, P. B. Radha, P. W. McKenty, J. D. Zuegel, F. J. Marshall, S. P. Regan, T. C. Sangster, W. Seka, E. M. Campbell, V. N. Goncharov, M. W. Bowers, J.-M. G. Di Nicola, G. Erbert, B. J. MacGowan, L. J. Pelz, J. Moody, and S. T. Yang, Phys. Plasmas **25**, 056314 (2018).

[74] B. M. Haines, F. F. Grinstein, and J. R. Fincke, Phys. Rev. E **89**, 053302 (2014).

[75] B. M. Haines, R. E. Olson, W. Sweet, S. A. Yi, A. B. Zylstra, P. A. Bradley, F. Elsner, H. Huang, R. Jimenez, J. L. Kline, C. Kong, G. A. Kyrala, R. J. Leeper, R. Paguio, S. Pajoom, R. R. Peterson, M. Ratledge, and N. Rice, Phys. Plasmas **26**, 012707 (2019).

[76] A. MacPhee, D. T. Casey, D. S. Clark, S. Felker, J. E. Field, S. W. Haan, B. A. Hammel, J. Kroll, O. L. Landen, D. A. Martinez, P. Michel, J. Milovich, A. Moore, A. Nikroo, N. Rice, H. F. Robey, V. A. Smalyuk, M. Stadermann, and C. R. Weber, Phys. Rev. E **95**, 031204(R (2017).